AGU PUBLICATIONS

Water Resources Research

RESEARCH ARTICLE
10.1002/2017WR021110

Key Points:
- Denitrification and sulfate reduction in beach aquifers are strongly affected by hydrology and physical characteristics of beaches
- Sandy beaches can attenuate 100% of land-derived nitrate prior to discharge
- Mixing-dependent reactivity increases primarily with the size of the mixing zone, mixing-independent reactivity increases with solute supply

Supporting Information:
- Supporting Information S1
- Supporting Information S2

Correspondence to:
H. A. Michael,
hmichael@udel.edu

Citation:
Heiss, J. W., Post, V. E. A., Laattoe, T., Russoniello, C. J., & Michael, H. A. (2017). Physical controls on biogeochemical processes in intertidal zones of beach aquifers. *Water Resources Research*, *53*. https://doi.org/10.1002/2017WR021110

Received 12 MAY 2017
Accepted 18 OCT 2017
Accepted article online 24 OCT 2017

Physical Controls on Biogeochemical Processes in Intertidal Zones of Beach Aquifers

James W. Heiss[1,2], Vincent E. A. Post[3,4], Tariq Laattoe[3], Christopher J. Russoniello[1], and Holly A. Michael[1,5]

[1]Department of Geological Sciences, University of Delaware, Newark, DE, USA, [2]Now at the National Academy of Sciences, Washington, DC, USA, [3]School of the Environment, National Centre for Groundwater Research and Training, Flinders University, Adelaide, SA, Australia, [4]Federal Institute for Geosciences and Natural Resources (BGR), Hannover, Germany, [5]Department of Civil and Environmental Engineering, University of Delaware, Newark, DE, USA

Abstract Marine ecosystems are sensitive to inputs of chemicals from submarine groundwater discharge. Tidally influenced saltwater-freshwater mixing zones in beach aquifers can host biogeochemical transformations that modify chemical loads prior to discharge. A numerical variable-density groundwater flow and reactive transport model was used to evaluate the physical controls on reactivity for mixing-dependent and mixing-independent reactions in beach aquifers, represented as denitrification and sulfate reduction, respectively. A sensitivity analysis was performed across typical values of tidal amplitude, hydraulic conductivity, terrestrial freshwater flux, beach slope, dispersivity, and DOC reactivity. For the model setup and conditions tested, the simulations demonstrate that denitrification can remove up to 100% of terrestrially derived nitrate, and sulfate reduction can transform up to 8% of seawater-derived sulfate prior to discharge. Tidally driven mixing between saltwater and freshwater promotes denitrification along the boundary of the intertidal saltwater circulation cell in pore water between 1 and 10 ppt. The denitrification zone occupies on average 49% of the mixing zone. Denitrification rates are highest on the landward side of the circulation cell and decrease along circulating flow paths. Reactivity for mixing-dependent reactions increases with the size of the mixing zone and solute supply, while mixing-independent reactivity is controlled primarily by solute supply. The results provide insights into the types of beaches most efficient in altering fluxes of chemicals prior to discharge and could be built upon to help engineer beaches to enhance reactivity. The findings have implications for management to protect coastal ecosystems and the estimation of chemical fluxes to the ocean.

1. Introduction

Nutrient loading from submarine groundwater discharge (SGD) can affect the health of nearshore marine ecosystems (Amato et al., 2016; LaRoche et al., 1997; Slomp & Van Cappellen, 2004; Valiela et al., 1997), leading to eutrophication, anoxic conditions, loss of habitat, and changes in the type and rate of primary production (Bowen et al., 2007; Paerl et al., 1998; Valiela et al., 1997). Fresh groundwater flowing from upland sources into coastal surface waters is often contaminated with nitrogen (N) in the form of NO_3^- from agricultural practices, oxidation of septic wastewater leachate, and leaky urban sewers in developed areas. Nutrient concentrations in groundwater are typically 2–3 orders of magnitude higher than in coastal surface waters (Slomp & Van Cappellen, 2004) and global SGD may rival surface runoff (Moore et al., 2008). Thus, SGD can serve as a significant pathway for nutrient delivery to estuaries and the coastal ocean (Burnett et al., 2007; Niencheski et al., 2007; Russoniello et al., 2016; Slomp & Van Cappellen, 2004; Taniguchi et al., 2008). However, the fate of nutrients prior to entering marine ecosystems is influenced by the temporal and spatial distribution of redox zones encountered along discharging flow paths (Charbonnier et al., 2013; Charette & Sholkovitz, 2002; Kroeger & Charette, 2008; McAllister et al., 2015; Reckhardt et al., 2015; Roy et al., 2011; Santoro, 2010; Santos et al., 2008; Slomp & Van Cappellen, 2004; Spiteri et al., 2008a). As the availability of reactive solutes needed to drive redox processes hinges upon the flow system, understanding how physical hydrogeologic characteristics influence the transport and transformation of nutrients in discharging groundwater is critical for effective management of nutrients for the protection of marine ecosystems.

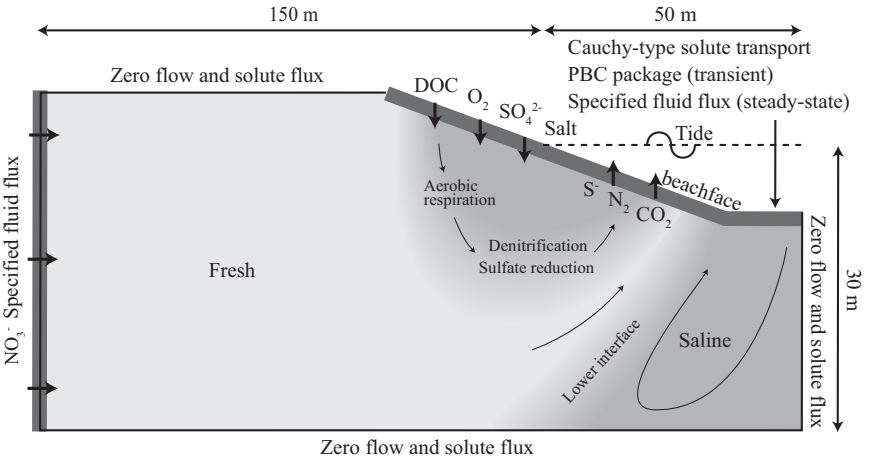

Figure 1. Conceptual and numerical model schematic showing reactants and products flowing into and out of the model domain, boundary conditions, and salinity distribution in a coastal aquifer.

Groundwater flow and solute transport in coastal aquifers leads to mixing between terrestrially derived fresh and marine-derived saline groundwater (Figure 1). Fresh groundwater driven by the inland hydraulic gradient flows into the beach aquifer and mixes with seawater infiltrating across the beachface due to tide (Abarca et al., 2013; Befus et al., 2013; Heiss & Michael, 2014; Michael et al., 2005; Robinson et al., 2006) and wave (Geng & Boufadel, 2015; Heiss et al., 2014; Robinson et al., 2014; Xin et al., 2014) action. The resulting hydraulic gradient leads to a pattern of circulating brackish to saline groundwater in the intertidal zone, where water flows downward from the high tide mark and seaward to discharge along the base of the beachface (Figure 1). The seaward extent of the brackish circulation cell is often, though not always (Evans & Wilson, 2016), bounded by a zone of fresh groundwater that discharges near the low tide mark. Farther seaward, density gradients drive circulation of saltwater along the lower saltwater-freshwater interface.

The intertidal zone hosts geochemical gradients that form as a result of mixing between the freshwater and saltwater end-members. These gradients drive microbially mediated chemical transformations that modify solute concentrations in groundwater prior to discharge. Chemical transformations in coastal aquifers include dissolved organic carbon (DOC) degradation (Kroeger & Charette, 2008), aerobic respiration (Slomp & Van Cappellen, 2004), denitrification (Meile et al., 2010; Santos et al., 2009), nitrification (Ullman et al., 2003), anaerobic ammonium oxidation (Slomp & Van Cappellen, 2004), dissimilatory NO_3^- reduction to ammonium (Santoro, 2010), sulfate reduction (McAllister et al., 2015), and iron oxidation (Charette & Sholkovitz, 2002). Iron oxidation leads to precipitation of iron oxides onto sediment surfaces that adsorb and sequester solutes including phosphate and arsenic along groundwater flow paths (Charette & Sholkovitz, 2002; Jung et al., 2009). Transformation of nitrate (NO_3^-) to N_2 gas via denitrification is a particularly important process for reducing the bioavailable N load to coastal waters (Galloway et al., 2003). Seawater infiltrating across the beachface due to wave and tidal action carries DOC and O_2 downward to the NO_3^--enriched freshwater beneath the intertidal zone (Anschutz et al., 2009; Kroeger & Charette, 2008; McAllister et al., 2015; Reckhardt et al., 2015; Santos et al., 2009; Ullman et al., 2003). Because O_2 is rapidly consumed as seawater circulates through the beach (Charbonnier et al., 2016), mixing between the DOC-rich seawater end-member and NO_3^--rich freshwater along deeper anaerobic flow paths will favor denitrification.

Sulfate (SO_4^{2-}) entering the beach with infiltrating seawater can serve as a terminal electron accepter once more efficient oxidizing agents are reduced. Reduction of SO_4^{2-} to sulfide (S^-) is important because S^- affects cycling of N and other elements. For example, denitrification can be fueled by oxidation of S^- rather than DOC (Rivett et al., 2008). Further, S^- reacts with Fe^{2+} to generate iron sulfide (FeS), leading to precipitation and FeS-coated sediments (McAllister et al., 2015). FeS minerals sequester different elements than iron oxides (Fan et al., 2013), hence understanding sulfate reduction and S^- distributions is a first step to understanding adsorption, precipitation, dissolution, and cycling of other chemicals in intertidal aquifers.

Nutrient concentrations in nearshore aquifers are spatially variable and tied to the physical mixing between the freshwater and saltwater end-members and the diagenetic recycling of DOC and POC (Gonneea &

Charette, 2014; Hays & Ullman, 2007; Kroeger & Charette, 2008; Reckhardt et al., 2015; Spiteri et al., 2008a; Ullman et al., 2003). Seasonal variability in the supply of freshwater and saltwater, and thus the supply of solutes to the reaction zone also affects the redox conditions of beach aquifers (Beck et al., 2008; Charbonnier et al., 2013; McAllister et al., 2015; Santos et al., 2008), as does the pH of the pore water (Spiteri et al., 2006). While the spatial and temporal patterns of biogeochemical reaction zones are becoming clearer, insight gained through field studies inherently considers the cumulative effects of multiple forcings acting on different time scales (e.g., Kim et al., 2017; Reckhardt et al., 2015). Compounded by the complexity of flow and transport in heterogeneous systems, cumulative and potentially nonlinear interactions mask the importance of the individual factors regulating nutrient cycling in these hydrologically and biogeochemically complex and dynamic coastal systems.

Numerical groundwater flow and reactive transport models can be used to investigate the individual physical controls on transport and chemical cycling in nearshore aquifers. Spiteri et al. (2008a, 2008b) demonstrated through modeling that nitrogen and phosphorous cycling along the lower saltwater-freshwater interface is controlled by the groundwater flow field and extent of mixing between saltwater and freshwater. Model sensitivity showed that denitrification was unable to remove large quantities of NO_3^- in systems with high groundwater velocities and low rates of DOC oxidation, leading to nearly conservative transport. Conversely, low groundwater velocities and high DOC oxidation rates increased denitrification rates and significantly reduced NO_3^- fluxes across the aquifer-ocean interface (Spiteri et al., 2008b). Meile et al. (2010) assessed the role of point-source septic systems as potential N sources by evaluating the importance of the freshwater gradient, DOC reactivity, and septic system setback distance on NO_3^- removal along the lower interface. Hydrologically more complex reactive transport models have demonstrated the importance of tides on regulating the fate of chemicals in coastal aquifers. Robinson et al. (2009) investigated the influence of tides on the degradation of benzene, toluene, ethylbenzene, and xylene (BTEX) in discharging groundwater and showed that an increase in tidal amplitude, a decrease in freshwater flux, and a decrease in the rate of O_2 consumption all increase BTEX removal. Anwar et al. (2014) simulated the effects of tides and waves on nutrient cycling and fluxes across the beachface and showed that NO_3^- attenuation increased with oceanic forcing (tidal and wave amplitude) due to greater mixing between saltwater and freshwater. In natural systems, oceanic forcing interacts with other physical factors that control NO_3^- attenuation, including beach slope, freshwater influx, hydraulic conductivity (K), and dispersion. However, the effects of these physical factors on NO_3^- and SO_4^{2-} attenuation in tidally influenced beach aquifers remain unclear. Additionally, changes to the distribution of denitrification rates, sulfate reduction rates, and reaction products beneath the intertidal zone in response to variation of these physical factors, including tidal amplitude, have not been investigated.

We assessed beach reactivity for mixing-dependent and mixing-independent reactions through simulation of denitrification and sulfate reduction, respectively. A mixing-dependent reaction requires that two solutes in different groundwater end-members mix to drive the reaction. Denitrification is considered a mixing-dependent reaction in intertidal sediments due to the presence of NO_3^- in coastal fresh groundwater and the prevalence of DOC in nearshore marine waters. A mixing-dependent reaction implies that all solutes required to drive the reaction are present in a single groundwater end-member. Sulfate reduction is modeled as a mixing-independent reaction as both DOC and SO_4^{2-} are present in seawater. Thus, in this study mixing between fresh and saline groundwater must take place for denitrification to occur, while sulfate reduction may take place in fully saline groundwater that does not undergo mixing.

Reactivity was assessed based on the amount of terrestrially derived NO_3^- and seawater-derived SO_4^{2-} removed prior to discharge. The size and location of the reaction zone and the distribution of dissolved species were also considered in our assessment. A sensitivity analysis of the five physical factors, tidal amplitude, freshwater flux, hydraulic conductivity, beach slope, and dispersivity, was performed over a range of typical values to identify the physical conditions that enhance beach reactivity. The results provide insight into the NO_3^- and SO_4^{2-} attenuation capacity of a wide spectrum of sandy beaches and reveal how the physical mechanisms controlling flow and transport alter the fate and fluxes of groundwater-borne nutrients to nearshore marine ecosystems.

2. Numerical Simulations

Groundwater flow, salt transport, and reactive solute transport in a beach aquifer was simulated using SEAWAT v4.0 (Langevin et al., 2007) and PHT3D v2.13 (Prommer & Post, 2002). SEAWAT v4.0 solves the coupled

flow and solute transport equations using a cell-centered finite difference approximation to simulate density-dependent groundwater flow and transport. PHT3D v.2.13 is a multispecies reactive transport model that uses output from SEAWAT v4.0 with the aqueous geochemical model PHREEQC-2 v2.17 (Parkhurst & Appelo, 1999) and the advective-dispersive multicomponent transport model MT3DMS (Zheng & Wang, 1999) to simulate chemical processes in flowing groundwater.

The model represented a cross section of a homogeneous, unconfined coastal aquifer with terrestrial freshwater inflow and saltwater inflow via tidal forcing. The model domain extended 50 m seaward and 150 m landward of the beachface-mean sea level (MSL) intersection and 30 m below MSL (Figure 1). A constant sloping beachface (0.069) was set along the aquifer-ocean interface. Following Robinson et al. (2007a, 2007b), a nonuniform grid with 125 layers and 184 columns was used, with higher discretization (dx = 0.31 m, dy = 0.06 m) in the intertidal zone where high groundwater flow rates, strong concentration gradients, and redox processes were present.

2.1. Groundwater Flow and Salt Transport Model

The boundary conditions for the flow and salt transport model were set to represent natural forcing conditions acting on a beach aquifer. Tidal forcing along the aquifer-ocean interface was simulated using the Periodic Boundary Condition (PBC) package (Post, 2011). A sinusoidal time-varying Dirichlet boundary condition was assigned to the aquifer-ocean interface nodes. The time-varying head was calculated as:

$$h_t = h_o + A\cos(\omega t - \theta) \quad (1)$$

where h_t (m rel. MSL) is the tidal elevation at time t, h_o (m) is a reference water level (MSL), A (m) is the tidal amplitude, ω ($=\frac{2\pi}{T}$) is the frequency in rad s^{-1}, and θ (rad) is the phase shift.

A Neumann boundary condition was set along the landward vertical boundary to represent freshwater inflow of terrestrial origin, with a constant salt concentration of 0 ppt. The top of the model domain landward of the shoreface, and the bottom, and right vertical boundaries were set as zero flow and zero salt flux. Model cells along the aquifer-ocean interface with inflowing seawater were assigned a constant salt concentration of 35 ppt, and a zero-concentration gradient was set for outward flow.

2.2. Reactive Transport Model

Microbially mediated biogeochemical processes occurring within beach aquifers were investigated using a reaction network of seven reactive species in two separate models. Together, the models consider DOC degradation, aerobic respiration, denitrification, and sulfate reduction, and include DOC, O_2, NO_3^-, N_2, CO_2, SO_4^{2-}, and S^- (Tables 1 and 2).

The first model simulates denitrification as a first-order reaction that requires mixing to occur as the inflow sources of NO_3^- and DOC are different. This was accomplished by assigning inflowing fresh groundwater along the left boundary as a source of NO_3^- and infiltrating seawater across the shoreface as a source of DOC. Thus, mixing between through-flowing fresh groundwater and circulating seawater in the beach aquifer was needed to drive the reaction. We omit the production of NH_4^+ from DOC mineralization and

Table 1
Reaction Network and Kinetic Rate Expressions

Reaction name	Reaction	Rate expression	β[a]
DOC degradation	DOC → no product	Rate = k_{fox}[DOC]	–
Aerobic respiration	$DOC + O_2 \rightarrow CO_2 + H_2O$	If $[O_2] >$ kmo2, Rate = k_{fox}[DOC]; if $[O_2] <$ kmo2, Rate = k_{fox}[DOC] ($[O_2]$/kmo2)	1
Denitrification	$5DOC + 4NO_3^- + 4H^+ \rightarrow 5CO_2 + 2N_2 + 7H_2O$	If $[O_2] >$ kmo2, Rate = 0; if $[O_2] <$ kmo2 and $[NO_3^-] >$ kmno3, Rate = k_{fox}[DOC] (1 – $[O_2]$/kmo2); if $[O_2] <$ kmo2 and $NO_3^- <$ kmo3, Rate = k_{fox}[DOC](1 – $[O_2]$/kmo2) ($[NO_3^-]$/kno3)	0.8
Sulfate reduction	$2DOC + SO_4^{2-} + H^+ \rightarrow HS^- + 2CO_2 + 2H_2O$	If $[O_2] >$ kmo2, Rate = 0; if $[O_2] <$ kmo2 and $[SO_4^{2-}] >$ kmso4, Rate = k_{fox}[DOC] (1 –$[O_2]$/kmo2); if $[O_2] <$ kmo2 and $SO_4^{2-} <$ kmso4, Rate = k_{fox}[DOC] (1 – $[O_2]$/kmo2) ($[SO_4^{2-}]$/kmso4)	0.5

Note. DOC degradation, aerobic respiration, denitrification, and sulfate reduction adopted or modified from Bardini et al. (2012).
[a]See supporting information.

Table 2
Reaction Parameter Values

Parameter	Units	Description	Value
k_{fox}	s^{-1}	Rate constant for decomposition of DOC	1.5×10^{-6} [a]
kmo2	M	Limiting concentration of O_2	3.125×10^{-5} [a,b]
kmno3	M	Limiting concentration of NO_3^-	8.065×10^{-6} [a,b]
kmso4	M	Limiting concentration of SO_4^{2-}	3.0×10^{-5} [c]

[a]Van Cappellen and Wang (1996).
[b]Bardini et al. (2012).
[c]Hunter et al. (1998).

subsequent nitrification as we are interested in quantifying NO_3^- transformation of land-derived sources only, and we discuss the implications of this omission in section 4.3.

The second model simulates sulfate reduction as a first-order reaction that does not require mixing. In this model, DOC and SO_4^{2-} both entered the beach with seawater due to tidal action. As a first-order reaction with both reactants entering across the beachface, SO_4^{2-} can transform to S^- once O_2 is depleted in the shallow subsurface; this process does not require mixing.

The reaction networks and rate expressions for DOC degradation, aerobic respiration, denitrification, and sulfate reduction were adopted from Bardini et al. (2012) and are based on the redox kinetics in Hunter et al. (1998). The reactions are shown in Table 1, and the corresponding reaction parameter values are provided in Table 2. DOC oxidation is assumed to be a linear first-order reaction with respect to the DOC concentration, with O_2, NO_3^-, and SO_4^{2-} as the terminal electron acceptors. However, the favorability of NO_3^- over SO_4^{2-} as a terminal electron acceptor is not considered because denitrification and sulfate reduction are modeled separately. This is done in order to focus on differences between mixing-dependent and mixing-dependent reactions, and likely has little impact on the results because the regions where the transformations occur are physically separated. The reduction of O_2 and NO_3^- proceeds from the more (O_2) to less (NO_3^-) thermodynamically favorable terminal electron acceptor in the denitrification model, and the reduction of O_2 and SO_4^{2-} proceeds from the more (O_2) to less (SO_4^{2-}) favorable terminal electron acceptor in the sulfate reduction model. The stoichiometry of each reaction is accounted for using β (Table 1), the stoichiometric ratio between the moles of transferred electrons per mole of oxidized DOC and moles of the electrons acceptor. Both models follow a modified Monod kinetic formulation where the reduction rate is limited by the availability of the electron acceptor. The reader is referred to the supplemental material for a detailed description of stoichiometry and the modified Monod formulation. Aerobic respiration in both models is assumed a simple first-order reaction where the reduction rate is constant when the O_2 concentration is greater than the limiting value, whereas below the O_2 limiting concentration, the reduction rate is linearly proportional to the O_2 concentration.

Similar to conservative salt transport, a zero concentration gradient was set along the discharging portion of the aquifer-ocean interface for the reactive solutes and a source concentration was set for the inflowing portion. Source concentrations along the aquifer-ocean interface and landward boundary were assigned according to literature values that are characteristic of coastal sediment (Berner, 1981; van Cappellen & Wang, 1996). Seawater entering the model domain across the aquifer-ocean interface served as a source of DOC (2×10^{-3} *M*), O_2 (3.13×10^{-4} *M*), and SO_4^{2-} (0.028 *M*). The model was designed to allow these solutes to only enter the aquifer through tidally driven flow pathways across the beachface. Inflow of DOC, O_2, and SO_4^{2-} across the seabed seaward of the lower interface due to density-driven convection was omitted, as the focus of this study is on reactivity in the intertidal circulation cell. Fresh groundwater inflow from the landward boundary contained NO_3^- (1.29×10^{-4} *M*).

Simulations were performed in three steps. First, variable-density flow and salt transport were simulated explicitly under a phase-resolved oscillating tidal signal for 500 days to ensure that dynamic steady state had been reached with respect to hydraulic head and salt concentration. Second, tidally phase-averaged fluid fluxes and salt concentrations across the aquifer-ocean interface were used to simulate steady state groundwater flow and transport. Finally, the reactive solutes were superimposed on the phase-averaged flow field from step two and PHT3D was run for 500 days to allow the reactive solutes to reach equilibrium. Reactive transport was modeled using the phase-averaged flow field to improve numerical convergence for PHT3D.

Preliminary modeling results showed that phase-averaged flows (step 2) resulted in smaller mixing zones compared to phase-resolved flows (step 1) due to the absence of oscillatory flows and corresponding reduction in hydrodynamic dispersion. To correct for this effect, dispersivity for the phase-averaged base case model was adjusted manually and the size of the mixing zone was checked against the phase-resolved counterpart until the size of the mixing zones matched. The dispersivity value that resulted in the match was used in all of the phase-averaged models except the models that were used to investigate the effects of dispersion. The size of the mixing zone was calculated as the area between the 1 and 10 ppt salinity contours and is used to quantify the intensity of mixing on the boundary of the intertidal circulation cell. This salinity range was chosen based on where denitrification took place in the aquifer, as discussed in section 3.

2.3. Sensitivity Analysis

A total of 365 flow and reactive transport simulations were performed around a base case parameter set to assess the effects of tidal amplitude, freshwater flux (Q_f), K, beach slope, dispersivity, and DOC degradation rate on nutrient distributions and fluxes across the sediment-water interface.

The relative effectiveness of mass transport by advection and hydrodynamic dispersion in the intertidal circulation cell can be quantified using the Péclet number, $Pe = L/\alpha_L$, where L is a characteristic length scale of the system, taken as the length of the beachface [*L*], and α_L is the longitudinal dispersivity [*L*]. *Pe* was varied from 0.8 to 3.2 by adjusting longitudinal dispersivity. It is generally accepted that transport by advection dominates when $Pe > 2$ and dispersion dominates for $Pe < 2$.

The dimensionless Damköhler number (*Da*) relates the chemical reaction time scale to the transport time scale within and across systems (Zarnetske et al., 2012) and has been used to relate denitrification rates to advective transport rates (Briggs et al., 2015; Gu et al., 2007; Ocampo et al., 2006). *Da* is defined here as

$$Da = k_{fox} * V_s/Q_i \quad (2)$$

where k_{fox} is the rate constant for DOC degradation [T^{-1}] and V_s/Q_i is the saltwater residence time [*T*] in the intertidal circulation cell, where V_s [L^3] is the volume of the saltwater in the intertidal circulation cell, and Q_i [L^3/T] is the tidally averaged influx across the sediment-water interface per unit length of shoreline. A *Da* of 1 implies that the supply of reactive solutes is balanced by reactive demand. As *Da* increases over 1 through either a decrease in the advective transport rate or an increase in the reaction rate, solute supply is unable to match reactive demand and the system becomes advection limited. As advective transport increases or the reaction rate decreases, *Da* decreases and supply outpaces demand resulting in a system that is rate limited. Thus, $Da > 1$ corresponds to advection-limited systems while $Da < 1$ indicates rate-limited systems.

The *Da* for a set of parameters is unknown a priori because residence time is calculated within the simulations. Trial and error was used to establish a base case model where *Da* was approximately 1 and *Pe* equaled 2. Parametric sensitivity was conducted around the base case over which tidal amplitude (0.25–1.35 m), hydraulic conductivity (2–50 m/d), freshwater flux (0.4–4 m^3/d), beach slope (0.0375–0.1), dispersivity (1–7.5 m), and the DOC rate constant (1.5×10^{-5}–1.5×10^{-7} s^{-1}) were varied. In the base case scenario, the tidal amplitude = 0.75 m, K = 25 m/d, freshwater flux = 2 m^3/d, beach slope = 0.068, longitudinal dispersivity = 3.0 m, and the DOC rate constant = 1.5×10^{-6} s^{-1}. The transverse dispersivity ratio was 0.1 in all models.

Reactivity for denitrification was assessed based on the quantity of NO_3^- removed in the intertidal zone and the amount of NO_3^- removed as a percent of terrestrial influx. Removal was calculated as the difference between the total flux into the model domain across the landward boundary and the total flux across the aquifer-ocean interface, in moles per day. Reactivity for sulfate reduction was evaluated based on the quantity of SO_4^{2-} transformed, and the amount of SO_4^{2-} transformed as a percent of influx across the aquifer-ocean interface.

3. Results

3.1. Solute and Reactivity Distributions—Base Case

Tidal forcing across the aquifer-ocean interface in the base case scenario formed a saltwater circulation cell in the intertidal zone where saltwater infiltrated near the high tide mark, flowed downward and seaward, and then discharged near the low tide mark, consistent with previous field and numerical modeling studies (Figure 2a; Abarca et al., 2013; Boufadel, 2000; Heiss & Michael, 2014; Lebbe, 1999; Michael et al., 2005; Robinson et al., 2006). Infiltrating seawater served as a source of labile DOC and O_2 to the intertidal zone

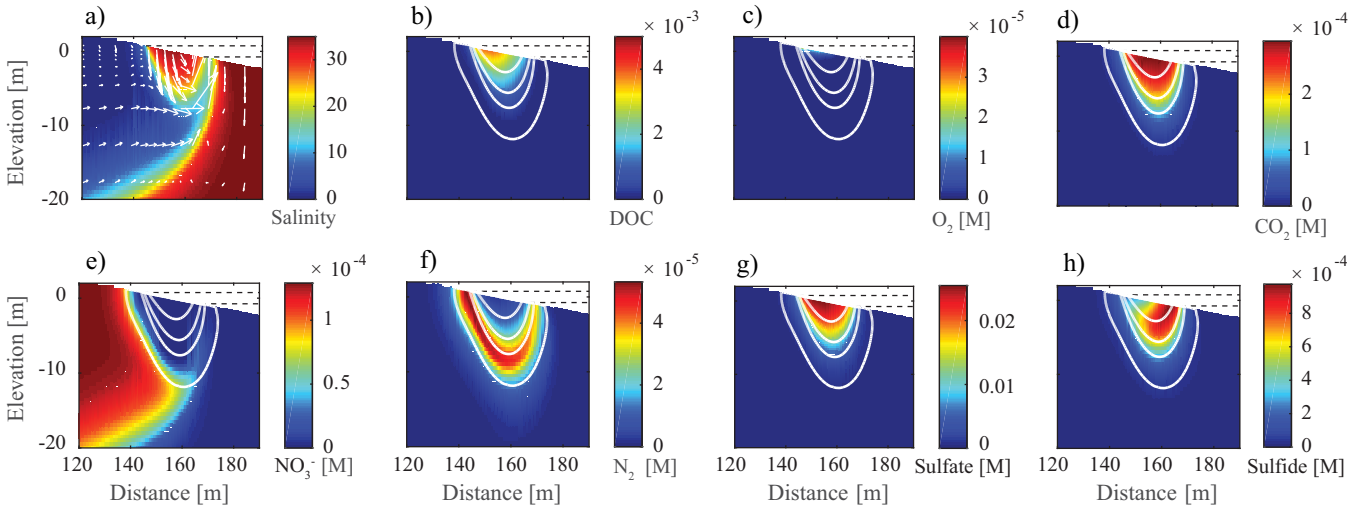

Figure 2. Solute distributions for the base case scenario. (a) Salinity and flow vectors, (b) DOC, (c) O_2, (d), CO_2, (e) NO_3^-, (f) N_2, (g) SO_4^{2-}, and (h) S^-. The 1, 10, 20, and 30 ppt salinity contours for the circulation cell are shown in Figures 2b–2g. The horizontal dashed lines are the high and low tide elevations.

leading to elevated DOC and O_2 concentrations immediately below the upper beachface (Figures 2b and 2c). The modeled O_2 distribution closely resembles the distribution measured by Charbonnier et al. (2016) and Kim et al. (2017), with concentrations decreasing with depth and distance seaward from the high tide mark. Aerobic respiration rates were highest immediately below the sand surface between the MSL-beachface intersection and the high tide mark because DOC and O_2 inputs were highest across that section of the beach (Figure 3a). Kim et al. (2017) conducted incubation experiments with pore water pumped from intertidal sediments and similarly found high aerobic respiration rates beneath the upper beachface. The modeled aerobic respiration rate decreased with depth as O_2 was depleted. This occurred immediately following the inflow of seawater into the intertidal aquifer, as indicated by the high CO_2 concentrations directly below the beach surface (Figure 2d). Once O_2 was completely consumed, the remaining DOC continued along flow paths and entered the mixing zone along the boundary of the circulation cell where it encountered NO_3^-. This led to anoxic conditions at depth and set up favorable conditions for denitrification.

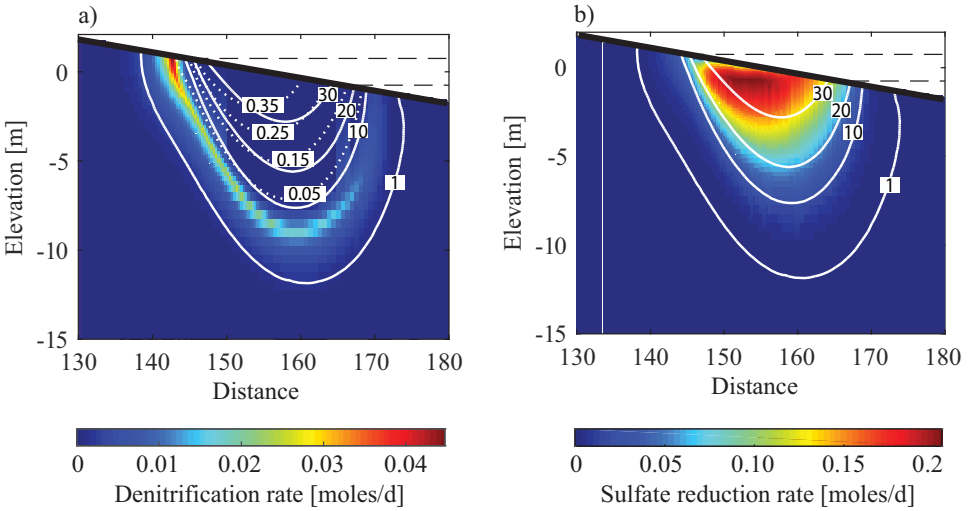

Figure 3. Reaction rates and zones for mixing-dependent and mixing-independent reactions. (a) Denitrification rate (colorbar), aerobic respiration rate (moles/d; dotted contours), and intertidal salinity (ppt; solid contours); (b) sulfate reduction rate (colorbar) and intertidal salinity (ppt; solid contours). Both plots show the base case. The horizontal dashed lines are the high and low tide elevations.

The reactants involved in denitrification, NO_3^- and DOC, originated in different waters; thus, the reaction was mixing dependent. The transition from aerobic respiration to denitrification occurred along the 10 ppt contour (Figure 3a). The denitrification rate was highest beneath the high tide mark and decreased along circulating flow paths to the low tide mark, forming an arc-shaped denitrification zone on the boundary of the circulation cell between 1 and 10 ppt, while aerobic respiration took place between 10 and 35 ppt. (Figure 3a). Thus, the aerobic respiration and denitrification zones were located on the inner and outer cell, respectively. Denitrification resulted in lower NO_3^- concentrations around the margins of the circulation cell than would occur due to conservative mixing (Figures 2a and 2e). N_2 was highest along the landward boundary of the saltwater circulation cell where denitrification rates were highest and decreased along circulating flow paths on the perimeter of the circulation cell (Figures 2f and 3a). These findings correlate well with the spatial pattern of N_2 concentrations derived from incubation experiments in Kim et al. (2017).

Since DOC and SO_4^{2-} both derive from the seawater that enters the beach, the reaction is not dependent on mixing with freshwater. SO_4^{2-} and S^- distributions reflect the reduction of SO_4^{2-} to S^- along circulating intertidal flow paths (Figures 2g and 2h). SO_4^{2-} entered the aquifer across the beachface due to tidal forcing and following rapid depletion of O_2, began to transform to S^-, which accumulated along circulating flow paths on the inside of the circulation cell (Figures 2g and 2h). Following first-order kinetics, the sulfate reduction rate was highest beneath the upper beachface where DOC and SO_4^{2-} concentrations were highest (Figure 3b). In the base case scenario and in the sensitivity tests, the sulfate reduction rate increased with increasing salinity and took place throughout the circulation cell, including in the mixing zone. The accumulation of S^- was highest along the 30 ppt salinity contour leading from the upper beachface to the low tide mark where the concentration of discharging S^- was highest. In contrast, N_2 accumulated along the 10 ppt salinity contour and discharged in a narrow zone 3 m seaward of the low tide mark. S^- was discharged farther landward because it was produced along shorter, more saline circulating flow paths while N_2 was produced in the deeper mixing zone and was thus transported farther seaward.

3.2. Sensitivity Analysis

3.2.1. Solute and Reactivity Distributions

Tidal amplitude, freshwater flux, K, and beach slope modified the location and rates of denitrification and sulfate reduction, and NO_3^-, N_2, SO_4^{2-}, and S^- concentrations in the intertidal zone. Hereafter, the part of the intertidal aquifer where NO_3^- was transformed to N_2 is defined as the denitrification zone, and the part of the beach where SO_4^{2-} was transformed to S^- is defined as the sulfate reduction zone.

The sizes of the reaction zones were most sensitive to tidal amplitude (Figure 4, row 1). As size of the mixing zone increased with tidal amplitude, the denitrification zone expanded and extended from the high tide mark, downward to the base of the circulation cell, and upward to the low tide mark. For tidal amplitudes below 0.55 m, the denitrification zone occupied the entire intertidal circulation cell. The sulfate reduction zone, indicated by the area inside the dashed white contour in Figure 4, expanded with the circulation cell as SO_4^{2-} flux across the beachface increased with tidal amplitude (Figure 4, row 1).

For low freshwater fluxes, the denitrification zone was located on the landward side of the mixing zone and did not extend to the discharge zone (Figure 4, row 2). Because the NO_3^- concentration along the left vertical boundary was constant across models, low freshwater fluxes resulted in lower NO_3^- fluxes. Therefore, all NO_3^- was consumed in a narrow band of denitrifying groundwater beneath the upper beachface. The thickness of the band increased with freshwater flux due to more dispersion and intensified mixing. Complete NO_3^- removal is evident by the absence of an NO_3^- discharge zone for cases with 0.5 and 1 m^3/d freshwater flux (Figure 5, row 2). The distribution of denitrification rates demonstrates that much of the removal for this case and other parameter sets with high amounts of removal occurred on the up-gradient side of the circulation cell (Figure 5, row 5). More seawater and SO_4^{2-} entered the aquifer at low freshwater fluxes and supported large sulfate reduction zones (Figure 4, row 2). Thus, the distribution of the sulfate reduction zone was controlled strictly by the flux of SO_4^{2-} across the beachface while the distribution of the denitrification zone was controlled by mixing and the supply of NO_3^- in freshwater.

The size of the denitrification and sulfate reduction zones increased with increasing K, but for different reasons (Figure 4, row 3). Higher K values resulted in larger mixing and wider denitrification zones due to increased hydrodynamic dispersion as a result of higher flow velocities. In contrast, the size of the sulfate reduction zone increased with K as more seawater and SO_4^{2-} infiltrated across the more permeable

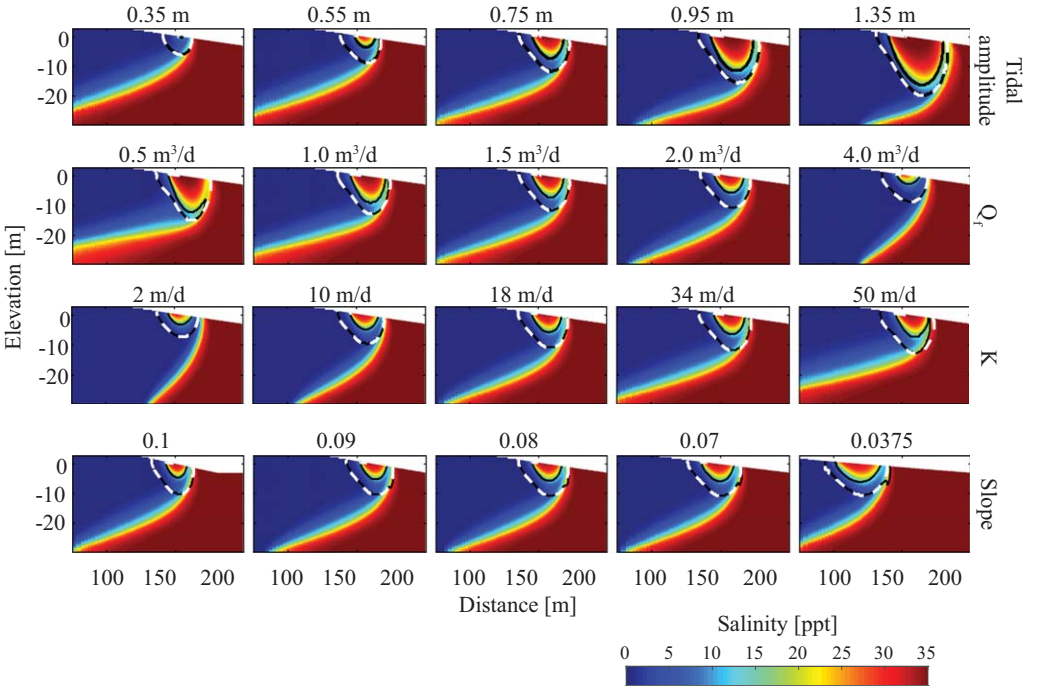

Figure 4. Denitrification zone (area between black contours) and sulfate reduction zone (dashed white contour) with varying tidal amplitude, freshwater flux, hydraulic conductivity, and beach slope. The base case scenario is the center plot in each row (A = 0.75 m, Q_f = 1.5 m^3/d, K = 18 m/d, slope = 0.08). The black and white contours are from two separate denitrification and sulfate reduction models, respectively.

beachface. Thus, K controlled the size of the denitrification zone through its effect on dispersion, and moderated the size of the sulfate reduction zone by influencing the infiltration rate.

Beach slope also affected the size and shape of the denitrification and sulfate reduction zones. The depths to the bottom of the circulation cell, denitrification zone, and sulfate reduction zone were constant across models while their horizontal extents almost doubled as the beach slope decreased (Figure 4, row 4). The thickness of the denitrification zone increased with increasing beach slope because steeper beaches supported stronger hydraulic gradients that enhanced dispersion and mixing. As the slope of the beach decreased, a larger tidal excursion led to a wider infiltration zone which allowed the sulfate reduction zone to expand horizontally.

N_2 concentrations were generally correlated with the distribution of denitrification rates. The highest N_2 concentrations were located on the landward side of the circulation cell where denitrification rates were highest and decreased along circulating flow paths due to dispersion. This is particularly evident for large tidal amplitudes, low freshwater fluxes, and high K values where longer flow paths and higher flow rates led to greater hydrodynamic dispersion and lower concentrations of discharging N_2 (Figure 5). In contrast, S^- was highest on the seaward side of the circulation cell for all model runs (Figure 6). N_2 produced in the narrow mixing zone dispersed transverse to circulating flow paths, so concentrations decreased toward the discharge zone. Dispersion of S^- was minimal because it was produced inside the circulation cell where advection dominated and instead accumulated to the point of discharge. The accumulation is most noticeable for large tidal amplitudes, low freshwater fluxes, high K values, and gentle sloping beachfaces (Figure 6).

In summary, the size and structure of the denitrification zone depended on the intensity of mixing and relative supply of NO_3^- and DOC, while the part of the beach undergoing sulfate reduction was tied to the supply of SO_4^{2-}.

3.2.2. Nitrate and Sulfate Attenuation

The five physical factors affected not only reaction rates and solute distributions, but also the magnitude of attenuation of land-derived NO_3^- and seawater-derived SO_4^{2-} in the intertidal zone. SO_4^{2-} transformation was significantly higher than NO_3^- removal on a molar basis due to the large quantity of SO_4^{2-} entering the

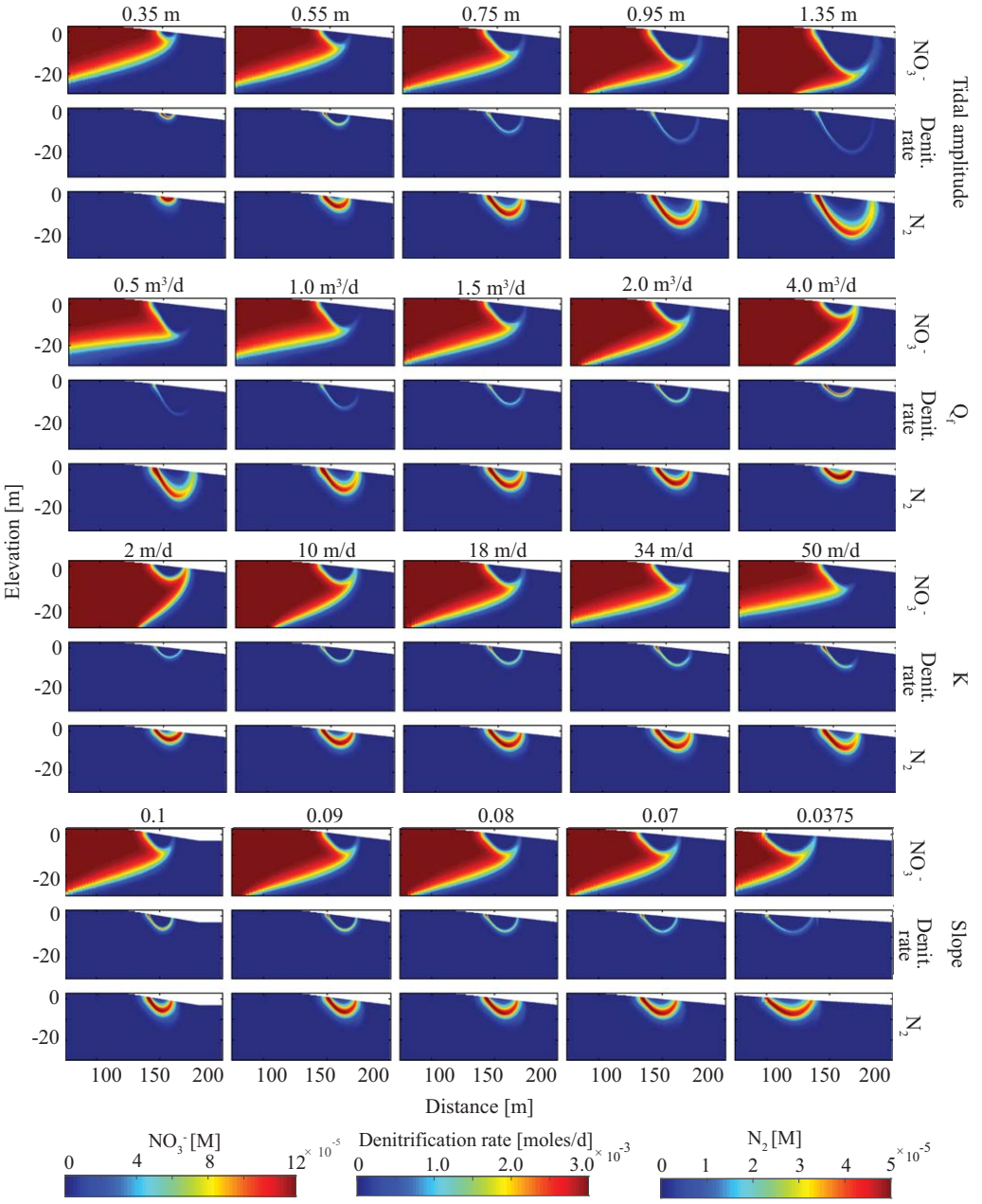

Figure 5. Denitrification rates and NO_3^- and N_2 concentrations for sensitivity to tidal amplitude, freshwater flux, hydraulic conductivity, and beach slope.

circulation cell with seawater (Figures 7 and 8). However, as a percentage of the SO_4^{2-} influx, sulfate transformation was low (0–7.5%; Figure 8), which is considerably less than for NO_3^- (0–100%; Figure 7).

Tidal amplitude significantly altered the total and percent NO_3^- removed prior to discharge. NO_3^- removal increased from 0% to 100% with increasing tidal amplitude up to 0.75 m as stronger tidal forcing created larger mixing zones (Figure 7a). For tidal amplitudes larger than 0.75 m ($Da = 1$), NO_3^- removal declined as the system became advection limited ($Da > 1$). The decline in reactivity was due to the reduction in the supply of DOC to the denitrification zone. As the size of the circulation cell grew, a larger proportion of DOC degraded along longer flow paths and less DOC reached the deeper sections of increasingly larger circulation cells. This reduced the supply of DOC to the mixing zone and resulted in a decline in total denitrification (Figure 7a) despite larger tidal amplitude producing larger mixing zones and increased DOC fluxes

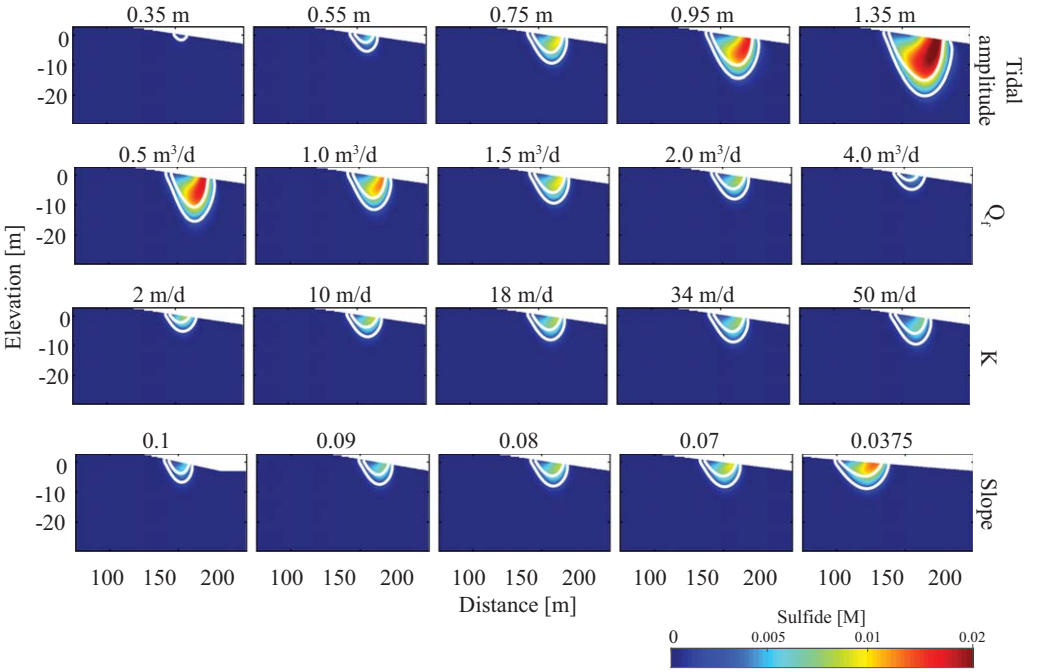

Figure 6. SO_4^{2-} (contours; 10% [inner] and 50% [outer] of maximum SO_4^{2-} concentration) and S^- (colorbar) concentrations for sensitivity to tidal amplitude, freshwater flux, hydraulic conductivity, and beach slope.

across the beachface. Consequently, large circulation cells do not always correlate with increased NO_3^- removal. A moderately sized tidal amplitude and mixing zone is optimal for NO_3^- removal due to the balance between the transport of DOC to the mixing zone and the size of the area with conditions suitable for

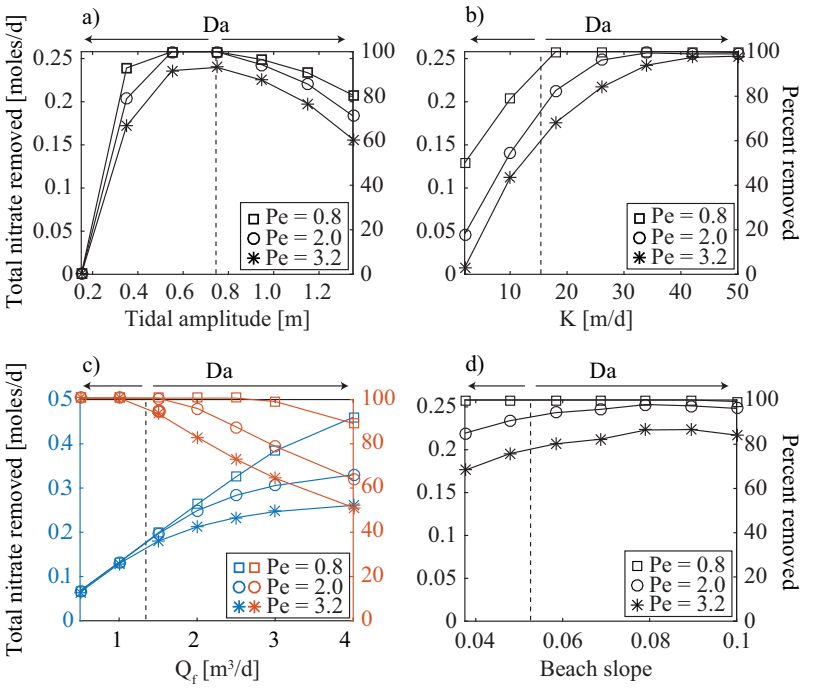

Figure 7. Sensitivity of total and percent NO_3^- removed to (a) tidal amplitude, (b) K, (c) freshwater flux, and (d) beach slope. Removal for 3 *Pe* values (solid lines) are shown for each physical parameter. The arrows along the top *x* axes indicates where *Da* is increasing (to the right) or decreasing (to the left) relative to *Da* = 1 (vertical dashed line). Total and percent removed are differentiated by color in Figure 7d because they do not correspond directly when NO_3^- flux into the model varies with freshwater flux.

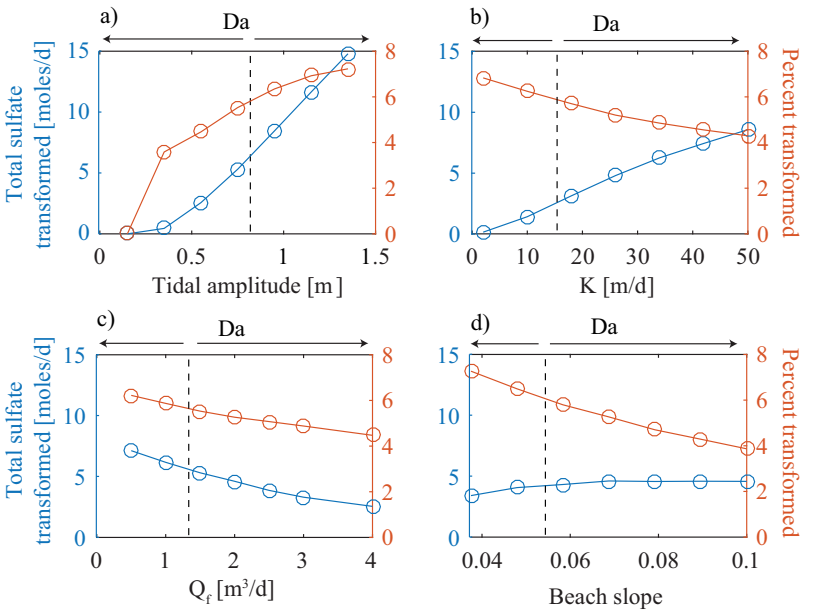

Figure 8. Sensitivity of total and percent sulfate transformed to (a) tidal amplitude, (b) K, (c) freshwater flux, and (e) beach slope. Results are shown for models with $Pe = 2$ for comparison to Figure 7. The arrows along the top x axes indicate where Da is increasing (to the right) or decreasing (to the left) relative to $Da = 1$ (vertical dashed line).

denitrification. Unlike denitrification, total and percent transformation of SO_4^{2-} increased monotonically with tidal amplitude (Figure 8a). Stronger tidal forcing introduced more SO_4^{2-} into the aquifer, increasing total transformation (supporting information Figure S4). The percent of inflowing sulfate that was transformed increased as a result of the lengthening residence times associated with large circulation cells and tidal amplitudes (supporting information Figure S3). Thus, beaches with tidal amplitudes that fall near the center (~0.75 m) of the tested range may host the highest mixing-dependent reactivity on a percentage basis, while larger tidal amplitudes may promote mixing-independent reactivity.

Hydraulic conductivity was the second most important physical factor controlling NO_3^- removal. NO_3^- removal increased from 20% to 100% as K increased from 2 to 50 m/d due to higher DOC fluxes and more dispersion resulting from higher flow velocities(Figure 7b, $Pe = 2$). Thus, despite high K values leading to shorter residence times that reduce reactivity, the effects of increased mixing and higher DOC fluxes dominated. The total amount of SO_4^{2-} transformed also increased with K (Figure 8b), however the increase was unrelated to mixing. Instead, the increase was due to higher fluxes of SO_4^{2-} entering the aquifer across more permeable beachfaces (supporting information Figure S4). This indicates that an increase in SO_4^{2-} supply was more important to the quantity of SO_4^{2-} transformed than short residence times resulting from high K values that act to reduce transformation. However, short residence times associated with high K values restricted the rate that total transformation could increase relative to influx, causing percent transformation to decline (Figure 8d).

High freshwater fluxes weakened tidally driven flows and resulted in small mixing zones. This led to a decrease in the percent of NO_3^- removed from 51 to 100% (Figure 7c, $Pe = 2$). NO_3^- was completely removed for low freshwater fluxes in large mixing zones. However, low freshwater fluxes did not result in the largest quantity of NO_3^- removed (Figure 7c). The quantity of NO_3^- removed was lowest for low freshwater fluxes because there was less available NO_3^- for consumption, while high freshwater fluxes supplied more NO_3^- to the mixing zone.

Variations in freshwater flux also modified sulfate reduction rates. High freshwater fluxes reduced the quantity of seawater and SO_4^{2-} infiltrating across the beachface which restricted the total amount of SO_4^{2-} transformed (Figure 8c). High freshwater fluxes also shortened intertidal residence times, which acted to reduce reactivity relative to additional influxes. Hence, sulfate transformation on a percentage basis also decreased with greater freshwater inflow.

The slope of the beach also affected NO_3^- attenuation with removal from 83 to 100% across beach slopes (Figure 7d, $Pe = 2$). Steep beaches supported stronger hydraulic gradients that increased dispersion and drove more DOC into the subsurface, increasing total and percent removal. In contrast, total SO_4^{2-} transformation was largely unaffected by the slope of the beach (Figure 8d). Although steep beaches supplied more DOC and SO_4^{2-} to the aquifer, the effects of short residence times on reducing reactivity acted to balance, or reduce in the case of percent transformation, the effects of an increased supply of reactants. These responses indicate that steep beaches may promote reactivity for mixing-dependent reactions while potentially reducing reactivity for mixing-independent reactions.

Longitudinal and transverse dispersivity controlled the intensity of mixing between freshwater and saltwater along the boundary of the circulation cell. Large mixing zones formed for large longitudinal and transverse dispersivity values (low *Pe*) and led to higher denitrification rates, as expected (Figure 7). Dispersion had no impact on sulfate reduction rates (see section 4.1).

3.2.3. Effects of DOC Reactivity

To assess the importance of DOC reactivity on NO_3^- and SO_4^{2-} attenuation, the DOC rate constant was varied between 1.5×10^{-5} and 1.5×10^{-7} s^{-1} across the range of values for tidal amplitude, K, freshwater flux, and beach slope (Figure 9). The range of DOC rate constants used in this study are within the range of values reported in literature and encompass the values used in similar studies (Anwar et al., 2014; Hunter et al., 1998; Spiteri et al., 2008b).

With the exception of the lowest rate constant, NO_3^- removal increased as DOC reactivity decreased for the tested values of each physical factor (Figures 9a–9d). At low DOC rate constants, less DOC degraded along circulating flow paths and hence more labile DOC was transported to the mixing zone. At high DOC rate constants, rapid DOC degradation limited the supply of DOC to the mixing zone to drive denitrification. However, the lowest DOC rate constant, 1.5×10^{-7} s^{-1}, did not correspond to the largest amount of NO_3^- removed (Figure 9). In this case, the effect of a marginal increase in the supply of DOC to the mixing zone was less important than the low DOC rate constant in controlling bulk NO_3^- transformation.

Whereas the supply of DOC was more important than the rate constant for denitrification, the opposite was true for sulfate reduction. Greater quantities of SO_4^{2-} were transformed at high DOC rate constants because O_2 was more rapidly consumed in the shallow subsurface. This improved the conditions for sulfate

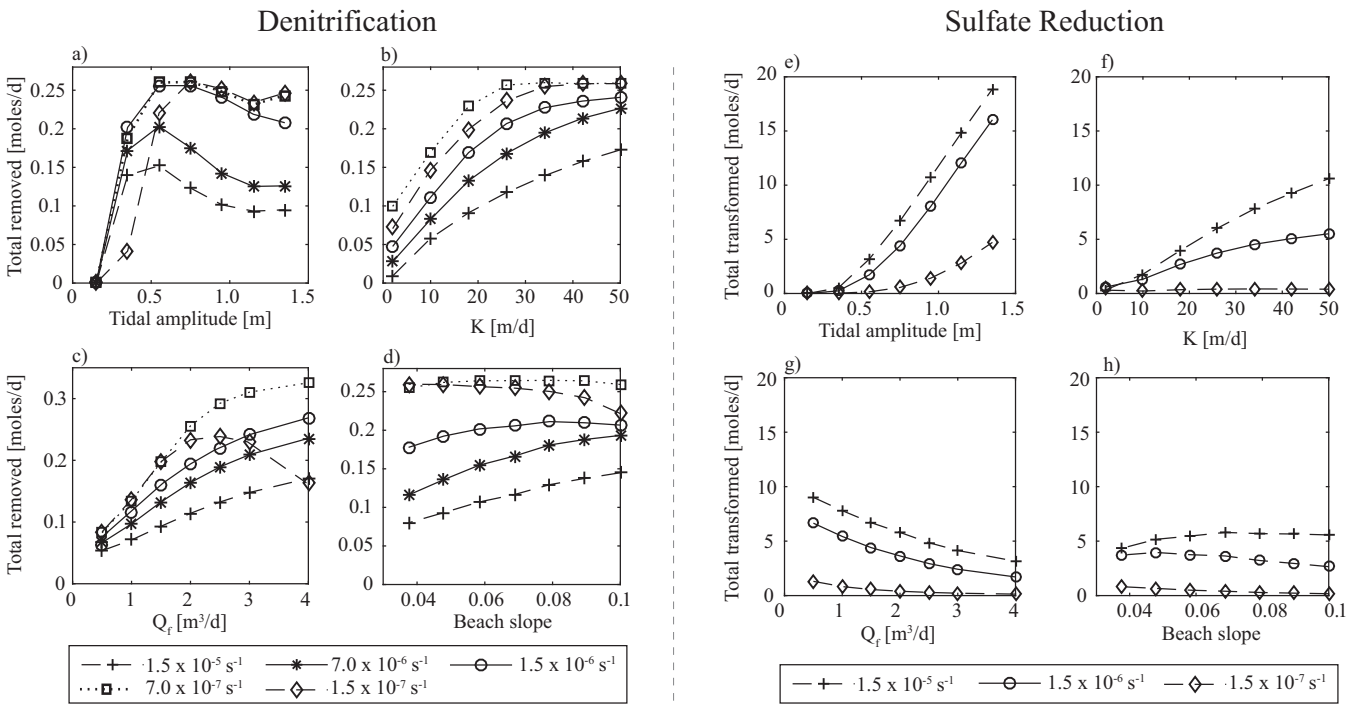

Figure 9. Total NO_3^- and SO_4^{2-} removed as a function of tidal amplitude, K, Q_f, and beach slope for a range of DOC rate constants.

reduction in the interior of the circulation cell since SO_4^{2-} was readily available as the next electron acceptor. For denitrification, aerobic respiration rates for all DOC rate constants were high enough that O_2 was fully consumed along the longer flow paths before reaching the mixing zone. The supply of DOC was therefore more important for denitrification, while the rate of O_2 consumption was the key factor in setting up favorable conditions for sulfate reduction over the range of tested DOC rate constants. The results demonstrate the importance of DOC reactivity on NO_3^- and SO_4^{2-} cycling in the intertidal zone and illustrate the influence of the interplay between the reaction rate and the physical flow system on nutrient transport and fate in beach aquifers.

4. Discussion

4.1. Physical and Biogeochemical Relationships

The simulations revealed relationships between the physical and chemical characteristics of the beach aquifer. The size of the mixing zone increased with the size of the circulation cell, representing an average of 79% of the circulation cell area (Figure 10a). The denitrification zone also increased with the size of the mixing zone and occupied an average of 49% of the mixing zone (Figure 10b), indicating that salinity alone is insufficient for identifying locations of NO_3^- removal. Although NO_3^- attenuation became more widespread in larger mixing zones, the mean reaction rate on a per-unit-area basis decreased as mixing intensified (Figure 10c). Large mixing zones denitrified a larger proportion of NO_3^-, and as removal approached 100%, the supply of reactants and hence mean reactivity on a per unit area basis declined. Thus, percent removal can be inferred based on the size of the mixing zone (Figure 10d). However, reactivity also depends on groundwater velocity, which governs residence time, the extent of mixing, and the rate of solute supply. Larger quantities of NO_3^- were removed as the average Darcy velocity, and thus mixing, in the intertidal zone increased (Figure 10e). Darcy velocity was primarily a function of freshwater flux, which also controlled the flux of NO_3^- to the circulation cell. The NO_3^- flux into the intertidal zone regulated the reactivity of the beach, and can be used to estimate the total quantity of NO_3^- attenuated in beach sediments for our model setup (Figure 10f).

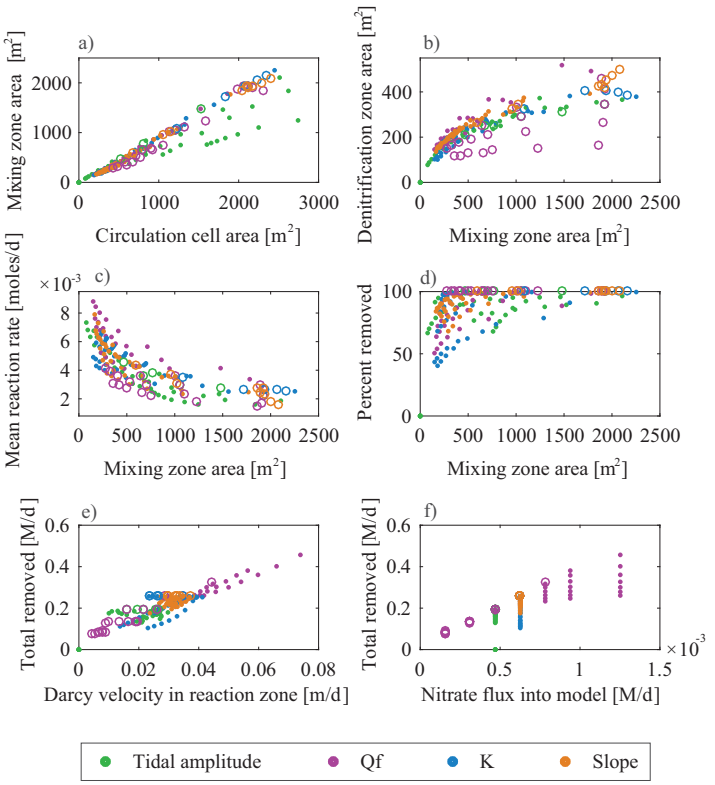

Figure 10. Relationships between phyiscal characteristics of the aquifer and denitrification.

Although Figure 10 demonstrates several relationships between physical characteristics and beach reactivity, there is no strong correlation between removal efficiency or total NO_3^- or SO_4^{2-} removed for many other parameters, including nondimensional numbers from literature that have successfully been used to predict physical properties of flow and transport in these systems (e.g., Evans & Wilson, 2016; Greskowiak, 2014; Robinson et al., 2007a, 2007b) (supporting information Figures S1–S4). The absence of correlations is owed to the competing effects of the physical factors on the flow and geochemical system. For example, as tidally driven circulation strengthens due to a decrease in freshwater flux, more DOC is introduced to the reaction zone that enhances reactivity, but where tidally driven circulation strengthens due to an increase in K, residence time in the circulation cell decreases and reactivity is reduced. Thus, tidally driven circulation is a poor metric for predicting NO_3^- removal (plots (a), supporting information Figures S1–S2). Similarly, a particular salinity gradient between the center of the circulation cell and the fresh discharge zone (i.e., Evans & Wilson, 2016) does not reflect the intensity of mixing on the boundary of the circulation cell and thus is a poor indication of NO_3^- and SO_4^{2-} removal (plots (c), supporting information Figures S1–S4). These two examples highlight the complexity of the interactions between the physical controlling factors and N cycling, many of which were not captured by the nondimensional numbers and other physical parameters.

Seven simulations were performed around the base case model to confirm that sulfate reduction proceeded independent of mixing

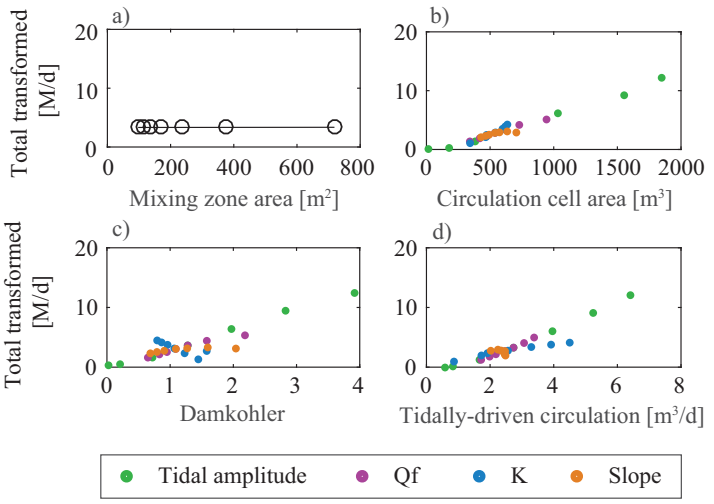

Figure 11. Relationships between phyiscal characteristics of the aquifer and sulfate reduction.

between freshwater and saltwater. This was accomplished by assigning a different dispersivity value to seven base case models (SEAWAT and PHT3D) to vary the intensity of mixing along the boundary of the circulation cell. Model results confirmed that in contrast to denitrification, the percent of SO_4^{2-} transformed was not correlated with the size of the mixing zone (Figure 11a), rather sensitivity tests on the effects of tidal amplitude, K, freshwater flux, and beach slope show that the amount of SO_4^{2-} transformed generally increased with the size of the circulation cell (Figure 11b). There was also a positive correlation between the amount of sulfate transformed and *Da* and tidally driven circulation (Figures 11c and 11d). The correlations between the size of the circulation cell, *Da*, and tidally driven circulation share a similar explanation. Greater quantities of SO_4^{2-} entered the beach with increasing tidally driven flow, which led to larger circulation cells, longer residence times, and hence larger *Da* values. Thus, the increase in total SO_4^{2-} transformed was due to an increase in supply of SO_4^{2-} and longer residence times.

4.2. Mixing-Dependent and Mixing-Independent Reactions

This study focused on the importance of five key physical factors and one biogeochemical factor controlling the reactivity of solutes involved in mixing-dependent and mixing-independent reactions. To test the importance of these controls, denitrification was modeled as an example first-order mixing-dependent reaction and sulfate reduction was modeled as an example first-order mixing-independent reaction. The variations in flow and transport regimes caused by changes to each physical factor led to distinct reactivity patterns. Those patterns are used here to identify the set of hydrologic and hydrogeologic parameters that result in the most reactive beach for mixing-dependent and mixing-independent reactions as they are modeled in this study.

The interplay between mixing intensity, residence time, and solute supply for denitrification, a mixing-dependent reaction, as shown in this study demonstrates that a system with a moderate (0.75 m) tidal amplitude, high K, high freshwater flux, and a steep beach with high dispersion are likely to attenuate the largest quantity of land-derived NO^{3-} prior to discharge according to our model setup and simplified reaction kinetics. More complex reactive transport models that consider additional reactions that directly or indirectly affect denitrification, such as nitrification, phosphate production through DOC mineralization, and Fe oxidation, indicate that denitrification is also highest for a tidal amplitude of 0.75 m (Anwar et al., 2014). This suggests that our simplified reaction network sufficiently represents denitrification as it relates to sensitivity to the five physical controls, and that simplified reaction networks may be a useful approach for evaluating other mixing-dependent reactions.

Reactions that do not require mixing have physical controls that differ from reactions that require mixing. A large tidal amplitude, high K, and low freshwater flux will promote transformation of solutes involved in mixing-independent reactions. The results suggest that any combination of physical factors that results in the largest influx of reactive solutes across the beachface and produces the longest residence time will yield the most reactive beach for these types of reactions.

Hydrologic controls interact to affect residence time and thus the processing time of N in the system. Residence time can explain the proportion of NO_3^- denitrified in lakes, rivers, estuaries, and on continental shelves (Seitzinger et al., 2006). However, in complex beach groundwater systems, the intensity of mixing is the primary control on the proportion of NO_3^- denitrified (Figure 10d). In the case of sulfate reduction, a mixing-independent reaction, SO_4^{2-} transformation is governed simply by the flux of SO_4^{2-} in circulating seawater (Figure 11d). Without a requirement for mixing, SO_4^{2-} loading sets the upper limit on the amount of SO_4^{2-} available to be transformed.

The results may help in the understanding of the behavior of other mixing-dependent and mixing-independent reactions in beach aquifers. Other mixing-dependent reactions that take place in beach aquifers include nitrification (Ullman et al., 2003), anaerobic ammonium oxidation (Slomp & Van Cappellen, 2004), dissimilatory NO_3^- reduction to ammonium (Santoro, 2010), sulfate reduction (McAllister et al., 2015),

abiotic (Charette & Sholkovitz, 2002) and biotic (McAllister et al., 2015) Fe(II) oxidation, and Fe(III) reduction (McAllister et al., 2015). Ullman et al. (2003) also observed nitrification as a mixing-independent reaction set up by the mineralization of seawater-derived DOC to NH_4^+ in the circulation cell. In that study, infiltration of seawater provided a source of DOC and maintained the oxic conditions required for nitrification. The findings may also provide insight into other mixing-independent reactions, including radium and radon production as well as other radioactive decay processes (Sanial et al., 2017).

The effects of anthropogenic disturbances that modify one or more of the five physical factors should be considered when evaluating redox activity in beach aquifers. These disturbances include, but are not limited to, beach nourishment, scraping, dune building, construction of ponds, and land use changes. Such disturbances alter intertidal slope, terrestrial freshwater flux, and sediment permeability and distribution within the beach. For example, beach scraping lowers the beach slope and could reduce reactivity for mixing-dependent reactions. However, gently sloping beaches can simultaneously increase the proportion of solutes undergoing transformation in mixing-independent reactions. Furthermore, beach nourishment projects may produce a more homogenous aquifer, thus reducing mixing-dependent reactivity while not affecting mixing-independent reactions. Such alterations may also be used to engineer beaches to promote reactivity for different types of reactions. However, the hydrologic and biogeochemical linkages as demonstrated in study are complex (see section 4.3), and other controls on redox reactions that were not investigated in this study should be considered prior to implementing engineering practices. Nevertheless, the results suggest that beach managers should take into account the effects of human alterations on reactivity when formulating best coastal zone management practices.

4.3. Model Simplifications and Assumptions

The findings in this study are a function of the model setup, reaction network, and boundary conditions, and are applicable only for the set of tested parameters and model scenarios. However, model development was informed using published literature of measurement and modeling of the same hydrologic and biogeochemical processes investigated in this study. Thus, the results are likely a reasonable approximation for reactivity in natural beach systems over the range of values tested.

The highest average denitrification rate in the circulation cells for all simulations, 0.3 mmol m^{-2} d^{-1} (SD 0.02 mmol m^{-2} d^{-1}), is at the lower end of the range (0.1–5.9 mmol m^{-2} d^{-1}) for subtidal sediments (Huettel et al., 2014), and outside of the range for denitrification rates (2.1–9 mmol m^{-2} d^{-1}) in the Wadden Sea intertidal sandflat (Gao et al., 2012) and those estimated by Schutte et al. (2015) for a sandy beach (3.3–19 mmol m^{-2} d^{-1}). The lower NO_3^- consumption rates simulated in this study can be explained by several factors that are discussed in this section along with simplifying assumptions of our modeling approach.

We considered denitrification as the primary pathway for NO_3^- attenuation; however, alternative NO_3^- transformation mechanisms and other N cycling pathways may play a role in affecting fluxes of bioavailable N to the water column. We chose to omit N mineralization and nitrification, as the focus of this study is on the effects of physics on mixing-dependent and mixing-independent reactions, and denitrification satisfied the requirements of a mixing-dependent reaction. Nitrification increases the availability of NO_3^- for discharge and thus actual NO_3^- fluxes in SGD may be higher than our estimates in real-word systems. Where that is the case, our simulations would overestimate removal rates as a percentage of the combined DOC-derived and terrestrially derived NO_3^- flux through the intertidal zone. However, nitrification promotes denitrification by producing NO_3^- and lowering O_2 concentrations, and thus our models may be underestimating total and percent removal rates. In either case, NO_3^- loading supported by nitrification of ammonium produced by marine-derived DOC mineralization is recycled bioavailable N from surface water rereleased back into the marine ecosystem, and we are therefore confident that our results represent removal rates and NO_3^- fluxes central to altering net marine ecosystem productivity. Furthermore, dissimilatory NO_3^- reduction to ammonium (DNRA) occurs under the same redox conditions as denitrification and competes with denitrification as an additional NO_3^- reduction mechanism. Microbial oxidation of reduced sulfur (S^-), typically in the form of iron sulfide (pyrite), to SO_4^{2-} can also provide a viable electron donor for denitrification (Cardoso et al., 2006), as can oxidation of reduced Fe^{2+} (Korom, 1992). In sediments where labile DOC is limited, these alternative NO_3^- reduction processes may increase NO_3^- attenuation (Kelso et al., 1997; Korom, 1992; Moncaster et al., 2000; Robertson et al., 1996; Tesoriero et al., 2000). Last, the proportion of labile and refractory DOC in real-world systems will shift along groundwater flow paths due to microbial uptake, and the

resulting distribution of DOC constituents will likely affect biogeochemical transformation of solutes in coastal aquifers.

We assumed homogenous media in our models to provide a first-order estimate of the efficiency of shallow coastal aquifers in attenuating solutes involved in mixing-dependent and mixing-independent reactions. Nevertheless, heterogeneity can significantly increase NO_3^- removal in aquatic sediments (Sawyer, 2014). The geochemical model also assumed that pH was constant in space and time, however pH gradients can significantly affect nutrient cycling in the salt water-freshwater mixing zone of aquifers (Spiteri et al., 2006). Future models should therefore consider pH in mixing-dependent and mixing-independent reaction formulations.

Wave swash and setup, diurnal and spring-neap variability in tidal amplitude, seasonal variability in recharge, storm events, and climate cycles alter flow paths and residence times and control the extent and intensity of mixing in nearshore aquifers (Abarca et al., 2013; Anwar et al., 2014; Ataie-Ashtiani et al., 1999; Bakhtyar et al., 2013; Gonneea & Charette, 2014; Gonneea et al., 2013; Heiss & Michael, 2014; Heiss et al., 2014, 2015; Li et al., 1999; Michael et al., 2005; Robinson et al., 2007a, 2007b, 2014; Xin et al., 2014). These hydrologic forcing mechanisms operate across a wide range of temporal and spatial scales and interact to form complex and highly dynamic flow regimes and mixing patterns more complicated those brought about by the constant freshwater flux boundary and sinusoidal tidal signal used in this study. These transient processes increase mixing and hence mixing-dependent reactions, suggesting that our results represent a lower bound for NO_3^- removal. The oscillatory flows and movement of redox boundaries resulting from transient hydrologic forcing mechanisms are also likely to be important for determining the distribution and type of microbial communities in the aquifer. For example, if the length of time that microorganisms require to become active when conditions are favorable is longer than the interval of time over which the geochemical environment changes due to moving redox boundaries, then the rate of N and S cycling and other chemical transformations may be diminished. Alternatively, interaction between land-ocean hydrologic forcings may lead to more dispersed and stable mixing zones where denitrifying communities may thrive, enhancing NO_3^- removal (Santoro, 2010). The hydrologic system also affects the temperature distribution in intertidal sediments (Befus et al., 2013), which may also affect the fate of groundwater constituents.

Nutrient cycling along the lower saltwater-freshwater interface can attenuate nitrogen loads in submarine groundwater discharge (Anwar et al., 2014; Kroeger & Charette, 2008; Spiteri et al., 2008b). This study was designed to investigate mixing-dependent and mixing-independent reactions in the saltwater circulation cell and therefore omits biogeochemical processes occurring along the lower interface. Simultaneous consideration of nutrient transformations in the intertidal mixing zone and the lower interface should be addressed in future studies to put our estimates into context with nutrient transformations in other regions of the coastal aquifer.

5. Conclusion

Variable-density flow, solute transport, and biogeochemical models were used to conduct a sensitivity analysis on the effects of tidal amplitude, hydraulic conductivity, freshwater flux, beach slope, dispersivity, and DOC reactivity on nutrient cycling in tidally influenced beach saltwater-freshwater mixing zones. The importance of these key physical and biogeochemical factors on reactivity was assessed for a mixing-dependent and a mixing-independent reaction. To explore the linkages between hydrology and these two types of reactions, labile dissolved organic carbon, dissolved oxygen, nitrate, sulfate, nitrite, and sulfide, representing the primary chemical species involved in aerobic respiration, denitrification, and sulfate reduction, were simulated. The results demonstrate that variability in the five physical controls, in addition to DOC reactivity, can significantly modify fluxes of nitrate and sulfate to the coastal ocean for the model setup, boundary conditions, and reaction network considered.

The results are the first to show the distribution of denitrification and sulfate reduction rates in intertidal beach aquifers. Denitrification occurred at the boundary of the intertidal circulation cell in an arc-shaped denitrification zone of groundwater between 1 and 10 ppt salinity. Nitrate consumption was highest on the landward side of the circulation cell and decreased along circulating flow paths from the high to low tide marks. Sensitivity tests showed that the size of the mixing zone was the primary physical characteristic

controlling the proportion of nitrate removal relative to terrestrial influx, while the terrestrial supply of nitrate was important for total denitrification. In contrast, sulfate reduction took place on the inside of the circulation cell and was highest beneath the beach surface where seawater recharged the aquifer. Sulfate reduction was controlled primarily by the supply of sulfate entering the aquifer across the beachface and was unaffected by the intensity of mixing.

Nitrate and sulfate removal varied significantly over the range of real-world hydrologic and beach conditions tested. Tidal amplitude was the most important factor moderating nitrate transformation (0–100% removed), followed by hydraulic conductivity (40–100%), freshwater flux (51–100%), beach slope (68–100%), and dispersivity (82–100%). The relative proportion of sulfate reduction (0–7.5% of total influx) was significantly less than that of denitrification (0–100% of total influx) due to the high influx of seawater-derived sulfate intro the beach aquifer. Sulfate transformation was most affected by tidal amplitude (0–7.5% removal), followed by K (4–7% removed) and beach slope (4–7.5%) and freshwater flux (4.5–6%). The results demonstrate that mixing-dependent and mixing-independent reactions occur in different locations and have different hydrologic and hydrogeologic controls.

The size of the mixing zone and solute supply are positively correlated to mixing-dependent reactivity while solute supply and residence time are responsible for controlling reactivity for mixing-independent reactions. There is a lack of correlation between reactivity and numerous other physical characteristics and nondimensional numbers published in literature, emphasizing the complexity of the interactions between the physical and biogeochemical factors controlling nutrient removal in these systems.

The findings reveal the hydrologic conditions and aquifer characteristics that support the highest rates of denitrification and sulfate reduction in intertidal sediments, based on our model setup and the set of six controlling factors considered. Beaches can be engineered to promote reactivity to reduce groundwater nutrient loads; however, these ecosystem services may be damaged if the effects of the five physical factors are not considered. Thus, the results may be useful to coastal managers aiming to moderate nutrient loads to nearshore ecosystems.

Acknowledgments
The authors thank Mahfuzur Khan for his helpful comments and modeling insight. Suggestions and comments from three anonymous reviewers significantly improved this manuscript. This research was supported by National Science Foundation (NSF) grants EAR-1246554, EAR-0910756, and Delaware EPSCoR with funds from NSF EPS-0814251 and the State of Delaware. The data used to produce the results of this paper may be obtained from the corresponding author.

References

Abarca, E., Karam, H., Hemond, H. F., & Harvey, C. F. (2013). Transient groundwater dynamics in a coastal aquifer: The effects of tides, the lunar cycle, and the beach profile. *Water Resources Research*, *49*, 1–16. https://doi.org/10.1002/wrcr.20075

Anschutz, P., Smith, T., Mouret, A., Deborde, J., Bujan, S., Poirier, D., & Lecroart, P. (2009). Tidal sands as biogeochemical reactors. *Estuarine, Coastal and Shelf Science*, *84*(1), 84–90. https://doi.org/10.1016/j.ecss.2009.06.015

Anwar, N., Robinson, C., & Barry, D. A. (2014). Influence of tides and waves on the fate of nutrients in a nearshore aquifer: Numerical simulations. *Advances in Water Resources*, *73*, 203–213. https://doi.org/10.1016/j.advwatres.2014.08.015

Amato, D. W., Bishop, J. M., Glenn, C. R., Dulai, H., & Smith, C. M. (2016). Impact of submarine groundwater discharge on marine water quality and reef biota of Maui. *PLoS ONE*, *11*(11), e0165825. https://doi.org/10.1371/journal.pone.016582

Ataie-Ashtiani, B., Volker, R. E., & Lockington, D. A. (1999). Tidal effects on sea water intrusion in unconfined aquifers. *Journal of Hydrology*, *216*(1–2), 17–31. https://doi.org/10.1016/S0022-1694(98)00275-3

Bakhtyar, R., Brovelli, A., Barry, D. A., Robinson, C., & Li, L. (2013). Transport of variable-density solute plumes in beach aquifers in response to oceanic forcing, *Advances in Water Resources*, *53*, 208–224, https://doi.org/10.1016/j.advwatres.2012.11.09

Bardini, L., Boano, F., Cardenas, M. B., Revelli, R., & Ridolfi, L. (2012). Nutrient cycling in bedform induced hyporheic zones, *Geochimica et Cosmochimica Acta*, *84*(2012), 47–61. https://doi.org/10.1016/j.gca.2012.01.025

Beck, M., Dellwig, O., Liebezeit, G., Schnetger, B., & Brumsack, H. J. (2008). Spatial and seasonal variations of sulphate, dissolved organic carbon, and nutrients in deep pore waters of intertidal flat sediments. *Estuarine, Coastal and Shelf Science*, *79*(2), 307–316. https://doi.org/10.1016/j.ecss.2008.04.007

Befus, K. M., Cardenas, M. B., Erler, D. V., Santos, I. R., & Eyre, B. D. (2013). Heat transport dynamics at a sandy intertidal zone. *Water Resources Research*, *49*, 3770–3786. https://doi.org/10.1002/wrcr.20325

Berner, R. A. (1981). Authigenic minerals resulting from organic matter decomposition in modern sediments. *Fortschritte Der Mineralogie*, *59*, 117–135.

Boufadel, M. C. (2000). A mechanistic study of nonlinear solute transport in a groundwater–surface water system under steady state and transient hydraulic conditions. *Water Resources Research*, *36*(9), 2549–2565.

Bowen, J. L., Kroegar, K. D., Tomasky, G., Pabich, W. J., Cole, M. L., Carmichael, R. H., & Valiela, I. (2007). A review of land–sea coupling by groundwater discharge of nitrogen to New England estuaries: Mechanisms and effect. *Applied Geochemistry*, *22*, 175–191.

Briggs, M. A., Day-Lewis, F. D., Zarnetske, J. P., & Harvey, J. W. (2015). A physical explanation for the development of redox microzones in hyporheic flow. *Geophysical Research Letters*, *42*, 4402–4410. https://doi.org/10.1002/2015GL064200

Burnett, W. C., Wattayakorn, G., Taniguchi, M., Dulaiova, H., Sojisuporn, P., Rungsupa, S., & Ishitobi, T. (2007). Groundwater-derived nutrient inputs to the Upper Gulf of Thailand. *Continental Shelf Research*, *27*, 176–190.

Cardoso, R. B., Sierra-Alvarez, R., Flores, E. R., Gómez, J., & Field, J. A. (2006). Sulfide oxidation under chemolithoautotrophic conditions. *Biotechnology and Bioengineering*, *95*(6), 1148–1157.

Charbonnier, C., Anschutz, P., Deflandre, B., Bujan, S., & Lecroart, P. (2016). Measuring pore water oxygen of a high-energy beach using buried probes. *Estuarine, Coastal and Shelf Science*, *179*, 66–78. https://doi.org/10.1016/j.ecss.2015.12.004

Charbonnier, C., Anschutz, P., Poirier, D., Bujan, S., & Lecroart, P. (2013). Aerobic respiration in a high-energy sandy beach. *Marine Chemistry*, *155*, 10–21. https://doi.org/10.1016/j.marchem.2013.05.003

Charette, M. A., & Sholkovitz, E. R. (2002). Oxidative precipitation of groundwater-derived ferrous iron in the subterranean estuary of a coastal bay. *Geophysical Research Letters*, *29*(10), 1444. https://doi.org/10.1029/2001GL014512

Evans, T. B., & Wilson, A. M. (2016). Groundwater transport and the freshwater–saltwater interface below sandy beaches. *Journal of Hydrology*, *538*, 563–573. https://doi.org/10.1016/j.jhydrol.2016.04.014

Fan, D., Anitori, R. P., Tebo, B. M., & Tratnyek, P. G. (2013). Reductive sequestration of pertechnetate ($^{99}TcO_4^-$) by nano zerovalent iron (nZVI) transformed by abiotic sulfide. *Environmental Science & Technology*, *47*, 5302–5310. https://doi.org/10.1021/es304829z

Galloway, J. N., Aber, J. D., & Erisman, J. W. (2003). The nitrogen cascade. *BioScience*, *53*(4), 341–356.

Gao, H., Matyka, M., Liu, B., Khalili, A., Kostka, J. E., Collins, G., . . . Kuypers, M. M. M. (2012). Intensive and extensive nitrogen loss from intertidal permeable sediments of the Wadden Sea. *Limnology and Oceanography*, *57*(1), 185–198. https://doi.org/10.4319/lo.2012.57.1.0185

Geng, X., & Boufadel, M. C. (2015). Numerical study of solute transport in shallow beach aquifers subjected to waves and tides. *Journal of Geophysical Research: Oceans*, *120*, 1409–1428. https://doi.org/10.1002/2014JC010539

Gonneea, M. E., & Charette, M. A. (2014). Hydrologic controls on nutrient cycling in an unconfined coastal aquifer. *Environmental Science & Technology*, *48*, 14178–14185.

Gonneea, M. E., Mulligan, A. E., & Charette, M. A. (2013). Climate-driven sea level anomalies modulate coastal groundwater dynamics and discharge. *Geophysical Research Letters*, *40*, 2701–2706. https://doi.org/10.1002/grl.50192

Greskowiak, J. (2014). Tide-induced salt-fingering flow during submarine groundwater discharge. *Geophysical Research Letters*, *41*, 6413–6419. https://doi.org/10.1002/2014GL061184

Gu, C. H., Hornberger, G. M., Mills, A. L., Herman, J. S., & Flewelling, S. A. (2007). Nitrate reduction in streambed sediments: Effects of flow and bio- geochemical kinetics. *Water Resources Research*, *43*, W12413. https://doi.org/10.1029/2007WR006027

Hays, R. L., & Ullman, W. J. (2007). Dissolved nutrient fluxes through a sandy estuarine beachface (Cape Henlopen, Delaware, U.S.A.): Contributions from fresh groundwater discharge, seawater recycling, and diagenesis. *Estuaries and Coasts*, *30*(4), 710–724. https://doi.org/10.1007/BF02841967

Heiss, J. W., & Michael, H. A. (2014). Saltwater-freshwater mixing dynamics in a sandy beach aquifer over tidal, spring-neap, and seasonal cycles. *Water Resources Research*, *50*, 6747–6766. https://doi.org/10.1002/2014WR015574

Heiss, J. W., Puleo, J. A., Ullman, W. J., & Michael, H. A. (2015). Coupled surface-subsurface hydrologic measurements reveal infiltration, recharge, and discharge dynamics across the swash zone of a sandy beach. *Water Resources Research*, *51*, 8834–8853. https://doi.org/10.1002/2015WR017395

Heiss, J. W., Ullman, W. J., & Michael, H. A. (2014). Swash zone moisture dynamics and unsaturated infiltration in two sandy beach aquifers. *Estuarine, Coastal and Shelf Science*, *143*, 20–31. https://doi.org/10.1016/j.ecss.2014.03.015

Huettel, M., Berg, P., & Kostka, J. E. (2014). Benthic exchange and biogeochemical cycling in permeable sediments. *Annual Review of Marine Science*, *6*, 23–51. https://doi.org/10.1146/annurev-marine-051413-012706

Hunter, K. S., Wang, Y., & Van Cappellen, P. (1998). Kinetic modeling of microbially-driven redox chemistry of radionuclides in subsurface environments: Coupling transport, microbial metabolism and geochemistry. *Journal of Contaminant Hydrology*, *209*, 53–80. https://doi.org/10.1016/S0169-7722(00)00158-3

Jung, H. B., Charette, M. A., & Zheng, Y. (2009). Field, laboratory, and modeling study of reactive transport of groundwater arsenic in a coastal aquifer. *Environmental Science & Technology*, *43*, 5333–5338. https://doi.org/10.1021/es900080q

Kelso, B. H. L., Smith, R. V., Laughlin, R. J., & Lennox, S. D. (1997). Dissimilatory nitrate reduction in anaerobic sediments leading to river nitrite accumulation. *Applied and Environmental Microbiology*, *63*(12), 4679–4685.

Kim, K. H., Heiss, J. W., Michael, H. A., Cai, W.-J., Laattoe, T., Post, V. E. A., & Ullman, W. J. (2017). Spatial patterns of groundwater biogeochemical reactivity in an intertidal beach aquifer. *Journal of Geophysical Research: Biogeosciences*, *122*, 2548–2562. https://doi.org/10.1002/2017JG003943

Korom, S. F. (1992). Natural denitrification in the saturated zone: A review. *Water Resources Research*, *28*(6), 1657–1668.

Kroeger, K. D., & Charette, M. A. (2008). Nitrogen biogeochemistry of submarine groundwater discharge. *Limnology and Oceanography*, *53*(3), 1025–1039. https://doi.org/10.4319/lo.2008.53.3.1025

Langevin, C. D., Thorne, D. T., Dausman, A. M., Sukop, M. C., & Guo, W. (2007). *SEAWAT Version 4: A computer program for simulation of multi-species solute and heat transport* (Technical Report, U.S. Geological Survey Techniques and Methods Book 6, Chapter A22, 39 pp.). Reston, VA: U.S. Geological Survey.

LaRoche, J., Nuzzi, R., Waters, R., Wyman, K., Falkowski, P. G., & Wallece, D. W. R. (1997). Brown tides blooms in Long Island's coastal waters linked to interannual variability in groundwater flow. *Global Change Biology*, *3*, 397–410.

Lebbe, L. (1999). Parameter identification in fresh-saltwater flow based on borehole resistivities and freshwater head data. *Advances in Water Resources*, *22*(8), 791–806.

Li, L., Barry, D. A., Stagnitti, F., & Parlange, J.-Y. (1999). Submarine groundwater discharge and associated chemical input to a coastal sea. *Water Resources Research*, *35*(11), 3253–3259. https://doi.org/10.1029/1999WR900189

McAllister, S. M., Barnett, J. M., Heiss, J. W., Findlay, A. J., Macdonald, D. J., Dow, C. L., . . . Chan, C. S. (2015). Dynamic hydrologic and biogeochemical processes drive microbially enhanced iron and sulfur cycling within the intertidal mixing zone of a beach aquifer. *Limnology and Oceanography*, *60*(1), 329–345. https://doi.org/10.1111/lno.10029

Meile, C., Porubsky, W. P., Walker, R. L., & Payne, K. (2010). Natural attenuation of nitrogen loading from septic effluents: Spatial and environmental controls. *Water Research*, *44*(5), 1399–1408. https://doi.org/10.1016/j.watres.2009.11.019

Michael, H. A., Mulligan, A. E., & Harvey, C. F. (2005). Seasonal oscillations in water exchange between aquifers and the coastal ocean. *Nature*, *436*, 1145–1148.

Moncaster, S. J., Bottrell, S. H., Tellam, J. H., Lloyd, J. W., & Konhauser, K. O. (2000). Migration and attenuation of agrochemical pollutants: Insights from isotopic analysis of groundwater sulphate. *Journal of Contaminant Hydrology*, *43*(2), 147–163.

Moore, W. S., Sarmiento, J. L., & Key, R. M. (2008). Submarine groundwater discharge revealed by ^{228}Ra distribution in the upper Atlantic Ocean. *Nature Geoscience*, *1*, 309–311. https://doi.org/10.1038/ngeo183

Niencheski, L. F. H., Windom, H. L., Moore, W. S., & Jahnke, R. A. (2007). Submarine groundwater discharge of nutrients to the ocean along a coastal lagoon barrier, southern Brazil. *Marine Chemistry*, *106*, 546–561.

Ocampo, C. J., Oldham, C. E., & Sivapalan, M. (2006). Nitrate attenuation in agricultural catchments: Shifting balances between transport and reaction. *Water Resources Research*, *42*, W01408. https://doi.org/10.1029/2004WR003773

Paerl, H., Pinckney, J., Fear, J., & Peierls, B. (1998). Ecosystem responses to internal and watershed organic matter loading: Consequences for hypoxia in the eutrophying Neuse River Estuary, North Carolina, USA. *Marine Ecology Progress Series*, *166*, 17–25.

Parkhurst, D. L., & Appelo, C. A. J. (1999). *User's guide to PHREEQC (version 2)—A computer program for speciation, batch-reaction, one dimensional transport, and inverse geochemical calculations* (Water Resour. Invest. Rep. 99–4259). Washington, DC: U.S. Department of the Interior.
Post, V. E. A. (2011). A new package for simulating periodic boundary conditions in MODFLOW and SEAWAT. *Computers and Geosciences*, *37*(11), 1843–1849. https://doi.org/10.1016/j.cageo.2011.01.012
Prommer, H., & Post, V. (2002). *A reactive multicomponent transport model for saturated porous media*. Edinburgh, UK: Contaminated Land Assessment and Remediation Research Centre, The University of Edinburgh.
Reckhardt, A., Beck, M., Seidel, M., Riedel, T., Wehrmann, A., Bartholomä, A., . . . Brumsack, H.-J. (2015). Carbon, nutrient and trace metal cycling in sandy sediments: A comparison of high-energy beaches and backbarrier tidal flats. *Estuarine, Coastal and Shelf Science*, *159*, 1–14. https://doi.org/10.1016/j.ecss.2015.03.025
Rivett, M. O., Buss, S. R., Morgan, P., Smith, J. W. N., & Bemment, C. D. (2008). Nitrate attenuation in groundwater: A review of biogeochemical controlling processes. *Water Research*, *42*(16), 4215–4232. https://doi.org/10.1016/j.watres.2008.07.020
Robertson, W. D., Russell, B. M., & Cherry, J. A. (1996). Attenuation of nitrate in aquitard sediments of southern Ontario. *Journal of Hydrology*, *180*(1), 267–281.
Robinson, C., Brovelli, A., Barry, D. A., & Li, L. (2009). Tidal influence on BTEX biodegradation in sandy coastal aquifers. *Advances in Water Resources*, *32*(1), 16–28. https://doi.org/10.1016/j.advwatres.2008.09.008
Robinson, C., Gibbes, B., Carey, H., & Li, L. (2007a). Salt-freshwater dynamics in a subterranean estuary over a spring-neap tidal cycle. *Journal of Geophysical Research*, *112*, C09007. https://doi.org/10.1029/2006JC003888
Robinson, C., Gibbes, B., & Li, L. (2006). Driving mechanisms for groundwater flow and salt transport in a subterranean estuary. *Geophysical Research Letters*, *33*, L03402. https://doi.org/10.1029/2005GL025247
Robinson, C., Li, L., & Barry, D. A. (2007b). Effect of tidal forcing on a subterranean estuary. *Advances in Water Resources*, *30*(4), 851–865. https://doi.org/10.1016/j.advwatres.2006.07.006
Robinson, C., Xin, P., Li, L., & Barry, D. A. (2014). Groundwater flow and salt transport in a subterranean estuary driven by intensified wave conditions. *Water Resources Research*, *50*, 165–181. https://doi.org/10.1002/2013WR013813
Roy, M., Martin, J. B., Smith, C. G., & Cable, J. E. (2011). Reactive-transport modeling of iron diagenesis and associated organic carbon remineralization in a Florida (USA) subterranean estuary. *Earth and Planetary Science Letters*, *304*(1–2), 191–201. https://doi.org/10.1016/j.epsl.2011.02.002
Russoniello, C. J., Konikow, L. F., Kroeger, K. D., Fernandez, C., Andres, A. S., & Michael, H. A. (2016). Hydrogeologic controls on groundwater discharge and nitrogen loads in a coastal watershed. *Journal of Hydrology*, *538*, 783–793.
Sanial, V., Buesseler, K. O., Charette, M. A., & Nagao, S. (2017). Unexpected source of Fukushima-derived radiocesium to the coastal ocean of Japan. *Proceedings of the National Academy of Sciences of the United States of America*, *114*, 11092–11096. https://doi.org/10.1073/pnas.1708659114
Santoro, A. (2010). Microbial nitrogen cycling at the saltwater-freshwater interface. *Hydrogeology Journal*, *18*, 187–202. https://doi.org/10.1007/s10040-009-0526-z
Santos, I. R., Burnett, W. C., Chanton, J., Mwashote, B., Suryaputra, I. G. N. A., & Dittmar, T. (2008). Nutrient biogeochemistry in a Gulf of Mexico subterranean estuary and groundwater-derived fluxes to the coastal ocean. *Limnology and Oceanography*, *53*(2), 705–718. https://doi.org/10.4319/lo.2008.53.2.0705
Santos, I. R., Burnett, W. C., Dittmar, T., Suryaputra, I. G N A., & Chanton, J. (2009). Tidal pumping drives nutrient and dissolved organic matter dynamics in a Gulf of Mexico subterranean estuary. *Geochimica et Cosmochimica Acta*, *73*(5), 1325–1339. https://doi.org/10.1016/j.gca.2008.11.029
Sawyer, A. H. (2014). Enhanced removal of groundwater-borne nitrate in heterogeneous aquatic sediments. *Geophysical Research Letters*, *42*, 403–410. https://doi.org/10.1002/2014GL062234
Schutte, C. A., Joye, S. B., Wilson, A. M., Evans, T., Moore, W. S., & Casciotti, K. (2015). Intense nitrogen cycling in permeable intertidal sediment revealed by a nitrous oxide hot spot. *Global Biogeochemical Cycles*, *29*, 1584–1598. https://doi.org/10.1002/2014GB005052
Seitzinger, S., Harrison, J. A., Böhlke, J. K., Bouman, A. F., Lowrance, R., Peterson, B., . . . Drecht, G. V. (2006). Denitrification across landscapes and waterscapes: A synthesis. *Ecological Applications*, *16*(6), 2064–2090.
Slomp, C. P., & Van Cappellen, P. (2004). Nutrient inputs to the coastal ocean through submarine groundwater discharge: Controls and potential impact. *Journal of Hydrology*, *295*, 64–86.
Spiteri, C., Regnier, P., Slomp, C. P., & Charette, M. A. (2006). pH-Dependent iron oxide precipitation in a subterranean estuary. *Journal of Geochemical Exploration*, *88*(1–3), 399–403. https://doi.org/10.1016/j.gexplo.2005.08.084
Spiteri, C., Slomp, C. P., Charette, M. A., Tuncay, K., & Meile, C. (2008a). Flow and nutrient dynamics in a subterranean estuary (Waquoit Bay, MA, USA): Field data and reactive transport modeling. *Geochimica et Cosmochimica Acta*, *72*(14), 3398–3412. https://doi.org/10.1016/j.gca.2008.04.027
Spiteri, C., Slomp, C., Tuncay, P. K., & Meile, C. (2008b). Modeling biogeochemical processes in subterranean estuaries: Effect of flow dynamics and redox conditions on submarine groundwater discharge of nutrients. *Water Resources Research*, *44*, W02430. https://doi.org/10.1029/2007WR006071
Taniguchi, M., Burnett, W. C., Dulaiova, H., Siringan, F., Foronda, J., Wattayakorn, G., . . . Ishitobi, T. (2008). Groundwater discharge as an important land-sea pathway into Manila Bay, Philippines. *Journal of Coastal Research*, *24*, 15–24.
Tesoriero, A. J., Liebscher, H., & Cox, S. E. (2000). Mechanism and rate of denitrification in an agricultural watershed: Electron and mass balance along groundwater flow paths. *Water Resources Research*, *36*(6), 1545–1559.
Ullman, W. J., Chang, B., Miller, D. C., & Madsen, J. A. (2003). Groundwater mixing, nutrient diagenesis, and discharges across a sandy beachface, Cape Henlopen, Delaware (USA). *Estuarine, Coastal and Shelf Science*, *57*, 539–552.
Valiela, I., McClelland, J., Hauxwell, J., Behr, P. J., Hersh, D., & Foreman, K. (1997). Macroalgal blooms in shallow estuaries: Controls and ecophysiological and ecosystem consequences. *Limnology and Oceanography*, *42*, 1105–1118.
Van Cappellen, P., & Wang, Y. (1996). Cycling of iron and manganese in surface sediments: A general theory for the coupled transport and reaction of carbon, oxygen, nitrogen, sulfur, iron, and manganese. *American Journal of Science*, *296*(3), 197–243. https://doi.org/10.2475/ajs.296.3.197
Xin, P., Wang, S. S. J., Robinson, C., Li, L., Wang, Y.-G., & Barry, D. A. (2014). Memory of past random wave conditions in submarine groundwater discharge. *Geophysical Research Letters*, *41*, 2401–2410. https://doi.org/10.1002/2014GL059617
Zarnetske, J. P., Haggerty, R., Wondzell, S. M., Bokil, V. A., & González-Pinzón, R. (2012). Coupled transport and reaction kinetics control the nitrate source-sink function of hyporheic zones. *Water Resources Research*, *48*, 1–15. https://doi.org/10.1029/2012WR011894
Zheng, C. M., & Wang, P. P. (1999). *MT3DMS. A modular three-dimensional multispecies transport model for simulation of advection, dispersion, and chemical reactions of contaminants in groundwater systems. Documentation and user's guide*. (Contract Rep. SERDP-99-1). Washington, DC: U.S. Army Corps of Engineers.